Nečas Center for Mathematical Modeling

Anisotropic hp-adaptive method based on interpolation error estimates in the Lq-norm

V. Dolejší

Preprint no. 2013-014

http://ncmm.karlin.mff.cuni.cz/

1

Abstract

We present a new anisotropic *hp*-adaptive technique, which can be employed for the numerical solution of partial differential equations in 2D with the aid of a discontinuous piecewise polynomial approximation. This method generates anisotropic triangular grids and the corresponding polynomial approximation degrees based on the minimization of the interpolation error in the L^q-norm ($q \in [1, \infty]$). We develop the theoretical background of this approach and present several numerical examples demonstrating the efficiency of the anisotropic adaptive strategy.

Anisotropic hp-adaptive method based on interpolation error estimates in the L^q-norm

Vít Dolejší[*]

1 Introduction

Adaptive methods exhibit an efficient tool for the numerical solution of partial differential equations (PDEs). An automatic mesh refinement or, more generally, an enhancement of the functional space where the approximate solution is sought, can significantly reduce the computational costs.

Among very efficient techniques belong the *hp-adaptive methods*, which allow the adaptation in the element size h as well as in the polynomial degree of approximation p. Based on many theoretical works, e.g., monographs [37, 35] or papers [5, 12, 39], we expect that the discretization error of a *hp*-method converges at an exponential rate in the number of degrees of freedom. Several *hp*-adaptive strategies have been proposed over the years, see, e.g., [29] or [22] for a survey. However, most of *hp*-adaptive methods deal with h-isotropic refinement when each element marked for h-refinement is split (isotropically) into several (usually four in 2D) daughter elements. Some exceptions are, e.g., [25, 34, 24], where quadrilateral elements can be split onto two daughter elements by a line in either the vertical or the horizontal directions.

On the other hand, many works (e.g., [2, 1, 3, 8, 13, 19, 21, 23, 26, 38, 42]) showed that *anisotropic elements* (i.e., long and thin triangles) are suitable in computation of problems with boundary or internal layers. The anisotropic element has shape extended in one dominant direction and it is characterized by three geometric features: the *size*, the *orientation*, and the *aspect ratio*. The orientation of the anisotropic element is the direction, along which its shape is extended, the size of the element corresponds to its diameter and the aspect ratio of the element is (roughly speaking) to the ratio between the size of the element and its "width". The anisotropic triangular grids are usually defined as grids consisting of equilateral triangles under a given Riemann metric.

The works mentioned above dealt mostly with first order finite volume or finite element methods. Thus the Hessian matrix (=matrix of the second order derivatives) is naturally employed for the definition of the Riemann metric. Furthermore, in [6, 7], the Riemann metrics (defining the optimal anisotropic mesh in the $W^{k,q}$-norm) were derived for the polynomial approximations of the higher degree (>1). This approach is based on a particular definition of the magnitude, orientation, and anisotropic ratio of the higher order derivatives of a function u, which characterize its anisotropic behaviour.

Our aim is to develop an efficient adaptive technique which employs both aspects mentioned above, i.e., it generates the so-called *anisotropic hp-grids*, where each element is characterized by its *size*, the *orientation*, the *aspect ratio*, and the *local polynomial approximation degree*. A *hp*-mesh is described by two functions: $\mathcal{M} : \Omega \to \mathrm{Sym}$ ($\Omega \subset \mathbb{R}^2$ is the computational domain and Sym is the space of 2×2 symmetric, positively definite matrices) and $\mathcal{P} : \Omega \to \mathbb{R}^+$ (= the set of positive real numbers). The function $\mathcal{M}$ represents the Riemann metric and thus defines a triangular grid. The function $\mathcal{P}$ defines the polynomial approximation degree on each triangle of this grid.

In this paper, we deal with the following *main problem*. Let $S_{h\mathsf{p}}$ denote the space of discontinuous piecewise polynomial functions uniquely defined for each *hp*-grid, cf. relation (2.2) bellow.

[*]This work was supported by grant No. 13-00522S of the Czech Science Foundation.

[*]Charles University Prague, Faculty of Mathematics and Physics, Sokolovská 83, 186 75 Praha, Czech Republic, dolejsi@karlin.mff.cuni.cz

For a given function u, we seek a *hp*-mesh such that
i) the *interpolation error* of a projection of u on $S_{h\mathsf{p}}$ in the L^q-norm ($q \in [1, \infty]$) is under a given tolerance,
ii) the dimension of $S_{h\mathsf{p}}$ (=*number of degrees of freedom*) is the smallest possible.

This problem exhibits a complicated task which we are not able to solve. Therefore, we define an auxiliary (local) problem whose solution will be heuristically employed for the solution of the main problem. Then the output of the presented considerations is the algorithm which generates, for a given u and a tolerance ω, the *hp*-mesh where the interpolation error is bounded by ω and the number of degrees of freedom is reasonably small (but not the smallest possible in general). This algorithm can be directly employed in the framework of the numerical solution of PDEs with the aid of the *discontinuous Galerkin method* (DGM), which is based on a discontinuous piecewise polynomial approximation.

The content of the rest of the paper is the following. In Section 2, we introduce basic notations and properties of anisotropic *hp*-meshes. Section 3 contains the definition of the main problem of this paper whose result is an optimal anisotropic *hp*-mesh. Moreover, we define and solve two auxiliary problems. In Section 4 we discuss the solution of the main problem and present the algorithm for a construction of the anisotropic *hp*-mesh. In Section 5 we describe the practical implementation of this algorithm and finally, Section 6 contains several numerical experiments demonstrating the efficiency of the proposed adaptive technique.

2 Anisotropic *hp*-meshes

We introduce the definition of *hp*-meshes with the aid of a matrix-valued function $\mathcal{M}$ (which we call the Riemann metric) and a function $\mathcal{P}$ (which we call the polynomial degree distribution function). The functions $\mathcal{M}$ and $\mathcal{P}$ are employed later for a practical construction of anisotropic *hp*-meshes.

2.1 Definition of *hp*-meshes

Let $\Omega \subset \mathbb{R}^2$ be a bounded computational domain with a polygonal boundary $\partial\Omega$. For simplicity, we assume that Ω is convex, however this assumption can be relaxed. By $\mathscr{T}_h = \{K\}$ ($h > 0$) we denote a conforming *triangulation* of Ω with standard finite element properties, see, e.g., [9] and $|K|$ is the area (= 2D Lebesgue measure) of $K \in \mathscr{T}_h$. Moreover, by $\mathscr{F}_h$ we denote the set of edges of $\mathscr{T}_h$. Here the edges $\boldsymbol{e} \in \mathscr{F}_h$ are considered as vectors from $\mathbb{R}^2$ given by its endpoints. The orientation of $\boldsymbol{e} \in \mathscr{F}_h$ is arbitrary.

Definition 2.1. Let $\mathscr{T}_h = \{K\}$ be a triangulation of Ω. To each $K \in \mathscr{T}_h$, we assign a positive integer p_K (=local polynomial approximation degree on K). Then we define the *polynomial degree vector* $\mathsf{p} := \{p_K;\ K \in \mathscr{T}_h\}$. Moreover, the pair

$$\mathscr{T}_{h\mathsf{p}} := \{\mathscr{T}_h, \mathsf{p}\} \tag{2.1}$$

is called the *hp-mesh*.

For the given *hp*-mesh $\mathscr{T}_{h\mathsf{p}}$, we construct the space of piecewise polynomial discontinuous functions by

$$S_{h\mathsf{p}} := \{v \in L^2(\Omega);\ v|_K \in P^{p_K}(K)\ \forall K \in \mathscr{T}_h\}, \tag{2.2}$$

where $P^{p_K}(K)$ is the space of polynomials of degree $\le p_K$ on $K \in \mathscr{T}_h$. The dimension of $P^{p_K}(K)$ is equal to $(p_K + 1)(p_K + 2)/2$ and the dimension of $S_{h\mathsf{p}}$ is

$$N_{h\mathsf{p}} := \sum_{K \in \mathscr{T}_h} (p_K + 1)(p_K + 2)/2. \tag{2.3}$$

We call $N_{h\mathsf{p}}$ the *number of degrees of freedom* of the *hp*-mesh $\mathscr{T}_{h\mathsf{p}}$. In order to proceed to the construction of anisotropic meshes, we introduce the anisotropy of triangles.

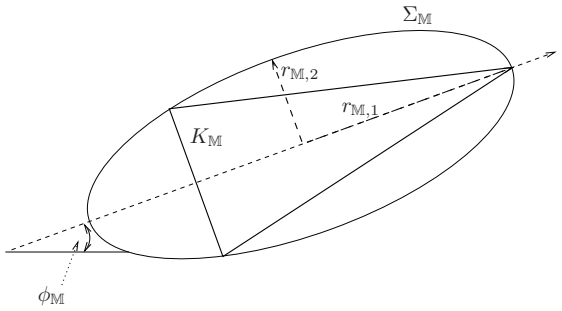

Fig. 1: The ellipse $\Sigma_{\mathbb{M}}$ with the length of semi-axes $r_{\mathbb{M},1}$, $r_{\mathbb{M},2}$ and the orientation $\phi_{\mathbb{M}}$, and the triangle $K_{\mathbb{M}}$ generated by $\mathbb{M}$ having the anisotropy $\{r_{\mathbb{M},1}, r_{\mathbb{M},1}/r_{\mathbb{M},2}, \phi_{\mathbb{M}}\}$.

2.2 Anisotropy of element

Similarly as in [6, 7], we define the anisotropy of a triangle with the aid of three parameters: the size, the aspect ratio and the orientation. We define the set of 2×2 symmetric and positively definite matrices

$$\mathrm{Sym} := \left\{ \mathbb{M} = \{m_{ij}\}_{i,j=1}^{2} \in \mathbb{R}^{2\times 2};\ m_{12} = m_{21},\ x^T \mathbb{M} x > 0\ \forall x \in \mathbb{R}^2,\ x \neq 0 \right\}, \tag{2.4}$$

where x^{T} denotes the row vector corresponding to the column vector $x = (x_1, x_2)$ and $x^{\mathrm{T}}\mathbb{M}x := m_{11}x_1^2 + 2m_{12}x_1x_2 + m_{22}x_2^2$.

Let $\mathbb{M} \in \mathrm{Sym}$. Then it can be decomposed in the form

$$\mathbb{M} = \begin{pmatrix} m_{11} & m_{12} \\ m_{12} & m_{22} \end{pmatrix} = \mathbb{Q}_{\phi_{\mathbb{M}}}^{\mathrm{T}} \begin{pmatrix} \lambda_{\mathbb{M},1} & 0 \\ 0 & \lambda_{\mathbb{M},2} \end{pmatrix} \mathbb{Q}_{\phi_{\mathbb{M}}}, \tag{2.5}$$

where $0 < \lambda_{\mathbb{M},1} \leq \lambda_{\mathbb{M},2}$ are the eigenvalues of $\mathbb{M}$, $\phi_{\mathbb{M}} \in [0, \pi)$, $\mathbb{Q}_\phi$ is the *rotation* through angle ϕ given by

$$\mathbb{Q}_\phi := \begin{pmatrix} \cos\phi & -\sin\phi \\ \sin\phi & \cos\phi \end{pmatrix} \tag{2.6}$$

and $\mathbb{Q}_{\phi_{\mathbb{M}}}^{\mathrm{T}}$ is the transpose matrix of $\mathbb{Q}_{\phi_{\mathbb{M}}}$.

Further, we put

$$\Sigma_{\mathbb{M}} := \left\{ x \in \mathbb{R}^2;\ x^{\mathrm{T}}\mathbb{M}x \leq 1 \right\}, \tag{2.7}$$

which defines the *ellipse* with the centre at origin, the semi-axes lengths

$$r_{\mathbb{M},1} := 1/\sqrt{\lambda_{\mathbb{M},1}}\ \geq\ r_{\mathbb{M},2} := 1/\sqrt{\lambda_{\mathbb{M},2}} \tag{2.8}$$

and the angle between the axis x_1 and the major axis of $\Sigma_{\mathbb{M}}$ is $\phi_{\mathbb{M}}$, see Figure 1.

Definition 2.2. Let $\mathbb{M} \in \mathrm{Sym}$ and $\Sigma_{\mathbb{M}}$ be the ellipse given by (2.7). Let $K_{\mathbb{M}}$ be an acute isosceles triangle which is inscribed into the ellipse $\Sigma_{\mathbb{M}}$ and which has the maximal possible area, see Figure 1. We say that $K_{\mathbb{M}}$ is *generated by the matrix* $\mathbb{M} \in \mathrm{Sym}$, $K_{\mathbb{M}}$ is the *triangle corresponding to the ellipse* $\Sigma_{\mathbb{M}}$ and $\Sigma_{\mathbb{M}}$ is the *ellipse corresponding to the triangle* $K_{\mathbb{M}}$.

With the aid of techniques presented in [15] or [13, Section 3] we can prove that the base of $K_{\mathbb{M}}$ is equal to $\sqrt{3}\, r_{\mathbb{M},2}$ and its height is equal to $\frac{3}{2} r_{\mathbb{M},1}$. Thus, the areas of $K_{\mathbb{M}}$ and $\Sigma_{\mathbb{M}}$ read

$$\begin{aligned} |K_{\mathbb{M}}| &= \frac{3\sqrt{3}}{4} r_{\mathbb{M},1} r_{\mathbb{M},2} = \frac{3\sqrt{3}}{4\sqrt{\lambda_{\mathbb{M},1}\lambda_{\mathbb{M},2}}} = \frac{3\sqrt{3}}{4\sqrt{\det \mathbb{M}}}, \\ |\Sigma_{\mathbb{M}}| &= \pi r_{\mathbb{M},1} r_{\mathbb{M},2} = \frac{\pi}{\sqrt{\lambda_{\mathbb{M},1}\lambda_{\mathbb{M},2}}} = \frac{\pi}{\sqrt{\det \mathbb{M}}}. \end{aligned} \tag{2.9}$$

Now, we are ready to define the anisotropy of a triangular element.

Definition 2.3. Let $K_{\mathbb{M}}$ be the triangle generated by $\mathbb{M} \in \mathrm{Sym}$. Let $r_{\mathbb{M},i},\ i = 1, 2$ are given by (2.8) and $\phi_{\mathbb{M}}$ by (2.5). We say that $r_{\mathbb{M},1}$ is the *size* of $K_{\mathbb{M}}$, $\sigma_{\mathbb{M}} := \frac{r_{\mathbb{M},1}}{r_{\mathbb{M},2}} \geq 1$ is the *aspect ratio* of $K_{\mathbb{M}}$ and $\phi_{\mathbb{M}}$ is the *orientation* of $K_{\mathbb{M}}$. Moreover, the triple $\{r_{\mathbb{M},1}, \sigma_{\mathbb{M}}, \phi_{\mathbb{M}}\}$ defines the *anisotropy* of $K_{\mathbb{M}}$. Furthermore, this triple defines also the *anisotropy of the ellipse* $\Sigma_{\mathbb{M}}$ given by (2.7). Hence, we speak also about the *size*, the *aspect ratio* and the *orientation* of the ellipse $\Sigma_{\mathbb{M}}$.

Remark 2.4. Let $r > 0$, $\sigma \geq 1$ and $\phi \in [0, 2\pi)$ be arbitrary. The triple $\{r, \sigma, \phi\}$ defines (in agreement with Definition 2.3) an anisotropic (acute isosceles) triangle K (and also the corresponding ellipse). Moreover, we can find a matrix $\mathbb{M}_K \in \mathrm{Sym}$ such that K is generated by $\mathbb{M}_K$.

Furthermore, let $\mathbb{M} \in \mathrm{Sym}$. We put

$$\|\boldsymbol{e}\|_{\mathbb{M}} := \left(\boldsymbol{e}^{\mathrm{T}}\mathbb{M}\boldsymbol{e}\right)^{1/2},\ \boldsymbol{e} = (e_1, e_2)^{\mathrm{T}} \in \mathbb{R}^2. \tag{2.10}$$

Obviously, the matrix $\mathbb{M}$ defines (by (2.10)) the *Riemann metric* in $\mathbb{R}^2$. The value $\|\boldsymbol{e}\|_{\mathbb{M}}$ is called the *size* of $\boldsymbol{e}$ *with respect* to $\mathbb{M}$. Finally, we recall one result from [13, Section 3].

Lemma 2.5. *Let* $\mathbb{M} \in \mathrm{Sym}$ *and* $K_{\mathbb{M}}$ *be the triangle generated by* $\mathbb{M}$. *Let* $\boldsymbol{e}_i^{K_{\mathbb{M}}},\ i = 1, 2, 3$ *denote the edges of* $K_{\mathbb{M}}$, *which are considered as vectors from* $\mathbb{R}^2$ *given by their endpoints. Then*

$$\|\boldsymbol{e}_i^{K_{\mathbb{M}}}\|_{\mathbb{M}} = \sqrt{3}, \quad i = 1, 2, 3. \tag{2.11}$$

Hence $K_{\mathbb{M}}$ *is equilateral with respect to* $\mathbb{M}$.

2.3 Riemann metric and the polynomial degree distribution function

In this section, we introduce the concept of the definition of the *hp*-mesh $\mathscr{T}_{h\mathsf{p}} = \{\mathscr{T}_h, \mathsf{p}\}$ from Definition 2.1 with the aid of a Riemann metric $\mathcal{M}$ and a polynomial degree distribution function $\mathcal{P}$. Similarly as in, e.g., [13, 19, 21, 23, 26, 38], the idea is to define an anisotropic triangular grid $\mathscr{T}_h$ as a mesh consisting of equilateral triangles with respect to a given Riemann metric.

Definition 2.6. Let $\mathcal{M} : \Omega \to \mathrm{Sym}$ be an integrable mapping. Moreover, let $\boldsymbol{v}_0, \boldsymbol{v}_1 \in \mathbb{R}^2$ be such that $\boldsymbol{v}_0 \in \Omega$ and $\boldsymbol{v}_0 + \boldsymbol{v}_1 \in \Omega$. The mapping $\boldsymbol{v} : [0, 1] \to \mathbb{R}^2$, $\boldsymbol{v}(t) = \boldsymbol{v}_0 + t\boldsymbol{v}_1,\ t \in [0, 1]$ parametrises a straight line in Ω between $\boldsymbol{v}_0$ and $\boldsymbol{v}_0 + \boldsymbol{v}_1$. Furthermore, we set

$$\|\boldsymbol{v}\|_{\mathcal{M}} := \int_0^1 \left(\boldsymbol{v}'(t)^{\mathrm{T}}\mathcal{M}(\boldsymbol{v}_0 + t\boldsymbol{v}_1)\boldsymbol{v}'(t)\right)^{1/2} \mathrm{d}t = \int_0^1 \left(\boldsymbol{v}_1^{\mathrm{T}}\mathcal{M}(\boldsymbol{v}_0 + t\boldsymbol{v}_1)\boldsymbol{v}_1\right)^{1/2} \mathrm{d}t. \tag{2.12}$$

We call $\mathcal{M}$ the *Riemann metric* on Ω and $\|\boldsymbol{v}\|_{\mathcal{M}}$ the *size* of edge $\boldsymbol{v}$ in the *Riemann metric* $\mathcal{M}$ (=distance between $\boldsymbol{v}_0$ and $\boldsymbol{v}_0 + \boldsymbol{v}_1$).

Remark 2.7. Let us note that if $\mathcal{M}$ is constant along $\boldsymbol{v}$ then (2.12) reduces to $\|\boldsymbol{v}\|_{\mathcal{M}} = (\boldsymbol{v}_1^{\mathrm{T}}\mathcal{M}\boldsymbol{v}_1)^{1/2}$ (compare with (2.10)). Moreover, if $\mathcal{M}(x) = \mathbb{I}\ \forall x \in \boldsymbol{v}$ ($\mathbb{I}$= the identity matrix) then $\|\boldsymbol{v}\|_{\mathcal{M}} = |\boldsymbol{v}|$ (=length of $\boldsymbol{v}$ in the Euclidean metric).

In virtue of (2.11), the aim is to define a mesh $\mathscr{T}_h$ such that

$$\|\boldsymbol{e}\|_{\mathcal{M}} = \sqrt{3} \quad \forall \boldsymbol{e} \in \mathscr{F}_h, \tag{2.13}$$

where $\mathscr{F}_h$ is the set of edges of $\mathscr{T}_h$. However, for the given metric $\mathcal{M}$, there does not exist (except special cases) any triangulation satisfying (2.13). Therefore, we define the triangulation *generated by metric* $\mathcal{M}$ such that the equalities (2.13) are satisfied approximately by the *least square technique*, see [13, 19]. Hence:

Definition 2.8. Let $\mathcal{M}$ be the Riemann metric on Ω. We say that the triangulation $\mathscr{T}_h$ of Ω is *generated by metric* $\mathcal{M}$ if

$$\mathscr{T}_h = \arg\min_{\mathscr{T}_h'} \sum_{\boldsymbol{e} \in \mathscr{F}_h'} \left(\|\boldsymbol{e}\|_{\mathcal{M}} - \sqrt{3}\right)^2, \tag{2.14}$$

where the minimum is taken over all possible triangulations $\mathscr{T}_h'$ of Ω and $\mathscr{F}_h'$ is the set of edges of $\mathscr{T}_h'$.

Let us note that there exist algorithms and codes, e.g., [33], [14], which construct mesh $\mathscr{T}_h$ for the given metric $\mathcal{M}$ in the sense of Definition 2.8.

Furthermore, the polynomial degree vector $\mathsf{p} = \{p_K;\ K \in \mathscr{T}_h\}$ can be defined in the following way.

Definition 2.9. Let $\mathcal{P} : \Omega \to \mathbb{R}^+$ be a given integrable function, which we call the *polynomial degree distribution function*. Moreover, let $\mathscr{T}_h$ be a triangulation of Ω, then using $\mathcal{P}$, we define the polynomial degree vector $\mathsf{p} = \{p_K;\ K \in \mathscr{T}_h\}$ from Definition 2.1 by

$$p_K := \operatorname{int}\left[\frac{1}{|K|}\int_K \mathcal{P}(x)\,\mathrm{d}x\right], \quad K \in \mathscr{T}_h, \tag{2.15}$$

where $\operatorname{int}[a] := \lfloor a + 1/2 \rfloor$ denotes the integer part of the number $a + 1/2,\ a \geq 0$.

We conclude that for the given Riemann metric $\mathcal{M} : \Omega \to \mathrm{Sym}$ and for the given polynomial degree distribution function $\mathcal{P} : \Omega \to \mathbb{R}^+$, there exists the unique *hp*-mesh $\mathscr{T}_{h\mathsf{p}} = \{\mathscr{T}_h, \mathsf{p}\}$ where $\mathscr{T}_h$ and p are given by Definitions 2.8 and 2.9, respectively.

Remark 2.10. Let $\mathcal{M} : \Omega \to \mathrm{Sym}$ and $\mathcal{P} : \Omega \to \mathbb{R}^+$ be given, and let $\mathscr{T}_{h\mathsf{p}} = \{\mathscr{T}_h, \mathsf{p}\}$ be the corresponding *hp*-mesh given by Definitions 2.8 and 2.9. Let $\bar{x} \in \Omega$ be arbitrary but fixed. Let $\bar{K} \in \mathscr{T}_h$ be such that $\bar{x} \in \bar{K}$ and let $p_{\bar{K}} \in \mathsf{p}$ be the corresponding polynomial approximation degree on $\bar{K}$. Moreover, let $K_{\bar{x}}$ be the triangle generated by $\mathcal{M}(\bar{x}) \in \mathrm{Sym}$ (in virtue of Definition 2.2). From the definition of $\mathscr{T}_{h\mathsf{p}}$, we expect that the anisotropies of triangles $K_{\bar{x}}$ and $\bar{K}$ are similar and also that $p_{\bar{K}}$ is close to $\mathcal{P}(\bar{x})$, i.e., there exist constants $\tilde{c}_1 \geq 1$ and $\tilde{c}_2 \geq 0$ independent of h and p such that

$$\begin{aligned} &\frac{1}{\tilde{c}_1} h_{K_{\bar{x}}} \leq h_{\bar{K}} \leq \tilde{c}_1 h_{K_{\bar{x}}}, && \frac{1}{\tilde{c}_1}\sigma_{K_{\bar{x}}} \leq \sigma_{\bar{K}} \leq \tilde{c}_1 \sigma_{K_{\bar{x}}}, \\ &|\phi_{K_{\bar{x}}} - \phi_{\bar{K}}| \leq \tilde{c}_2, && \frac{1}{\tilde{c}_1}\mathcal{P}(\bar{x}) \leq p_{\bar{K}} \leq \tilde{c}_1 \mathcal{P}(\bar{x}), \end{aligned} \tag{2.16}$$

where $\{h_{K_{\bar{x}}}, \sigma_{K_{\bar{x}}}, \phi_{K_{\bar{x}}}\}$ and $\{h_{\bar{K}}, \sigma_{\bar{K}}, \phi_{\bar{K}}\}$ are the anisotropies of $K_{\bar{x}}$ and $\bar{K}$, respectively. Therefore, the matrix $\mathcal{M}(\bar{x}) \in \mathrm{Sym}$ and the integer $\mathcal{P}(\bar{x})$ describe locally the *hp*-mesh $\mathscr{T}_{h\mathsf{p}}$ at $\bar{x}$.

In Section 4, we derive $\mathcal{M}$ and $\mathcal{P}$ such that the corresponding *hp*-mesh is optimal in the sense specified later. Let us note that in practice, it is sufficient to evaluate $\mathcal{M}$ and $\mathcal{P}$ only in a finite number of nodes $x \in \Omega$.

2.4 Generalized number of degrees of freedom

For the purpose of the construction of the anisotropic *hp*-meshes, it is suitable to introduce a quantity, which gives information about the number of degrees of freedom of the *hp*-mesh generated by the Riemann metric $\mathcal{M}$ and the polynomial degree distribution function $\mathcal{P}$.

First, we consider the following case. Let $\{\mathscr{T}_h, \mathsf{p}\}$ be a given *hp*-mesh of Ω. We define piecewise constant functions $\tilde{\nu} : \Omega \to (0, \infty)$ and $\tilde{d}(x) : \Omega \to \mathbb{N}$ (=set of all integers) by

$$\tilde{\nu}(x) := \begin{cases} |K| & \text{if } x \in \mathring{K} \text{ of some } K \in \mathscr{T}_h, \\ \text{arbitrary} & \text{if } x \in \partial K \text{ of some } K \in \mathscr{T}_h, \end{cases} \tag{2.17}$$

$$\tilde{d}(x) := \begin{cases} (p_K + 1)(p_K + 2)/2 & \text{if } x \in \mathring{K} \text{ of some } K \in \mathscr{T}_h, \\ \text{arbitrary} & \text{if } x \in \partial K \text{ of some } K \in \mathscr{T}_h, \end{cases} \tag{2.18}$$

where $|K|$ is the area of $K \in \mathscr{T}_h$, $\mathring{K}$ denotes the interior of $K \in \mathscr{T}_h$ and $p_K \in \mathsf{p}$ is the polynomial

approximation degree on $K \in \mathscr{T}_h$. We find that

$$\int_\Omega \frac{1}{\tilde{\nu}(x)}\,\mathrm{d}x = \sum_{K\in\mathscr{T}_h}\int_K \frac{1}{\tilde{\nu}(x)}\,\mathrm{d}x = \sum_{K\in\mathscr{T}_h}\int_K \frac{1}{|K|}\,\mathrm{d}x = \sum_{K\in\mathscr{T}_h} 1 = N_h, \tag{2.19}$$

$$\begin{aligned}\int_\Omega \frac{\tilde{d}(x)}{\tilde{\nu}(x)}\,\mathrm{d}x &= \sum_{K\in\mathscr{T}_h}\int_K \frac{\tilde{d}(x)}{\tilde{\nu}(x)}\,\mathrm{d}x = \sum_{K\in\mathscr{T}_h}\int_K \frac{(p_K+1)(p_K+2)/2}{|K|}\,\mathrm{d}x \\ &= \sum_{K\in\mathscr{T}_h}(p_K+1)(p_K+2)/2 = N_{h\mathsf{p}},\end{aligned} \tag{2.20}$$

where N_h is the number of triangles of $\mathscr{T}_h$ and $N_{h\mathsf{p}}$ is the number of degrees of freedom of $\mathscr{T}_{h\mathsf{p}}$ given by (2.3). Therefore, we interpret the function $\tilde{d}(x)/\tilde{\nu}(x)$ as the *"density of the number of degrees of freedom"*.

Our aim is to evaluate (at least approximately) the number of triangles of $\mathscr{T}_h$ and the number of degrees of freedom of $\mathscr{T}_{h\mathsf{p}}$ directly from functions $\mathcal{M}$ and $\mathcal{P}$. Let $\mathcal{M}:\Omega\to\mathrm{Sym}$ and $\mathcal{P}:\Omega\to\mathbb{R}^+$ be given and let $x\in\Omega$ be arbitrary but fixed. Then $\mathcal{M}(x)\in\mathrm{Sym}$ and let K_x denote the triangle generated by $\mathcal{M}(x)$ in virtue of Definition 2.2. Using (2.9), the area of K_x is $|K_x| = \frac{3\sqrt{3}}{4}\left(\det\mathcal{M}(x)\right)^{-1/2}$. Thus, we define the function

$$\nu(x) := \frac{3\sqrt{3}}{4}\left(\det\mathcal{M}(x)\right)^{-1/2}, \quad x\in\Omega, \tag{2.21}$$

which represents a generalization of the function ν from (2.17). Then, in virtue of (2.19), the value $\int_\Omega \nu(x)^{-1}\,\mathrm{d}x$ corresponds to the number of the triangles of $\mathscr{T}_h$ generated by the metric $\mathcal{M}$ in the sense of Definition 2.8.

Furthermore, we define the function

$$d(x) := \frac{1}{2}(\mathcal{P}(x)+1)(\mathcal{P}(x)+2), \quad x\in\Omega, \tag{2.22}$$

which represents a generalization of the function d from (2.18). Then, in virtue of (2.20), we define the *generalized number of degrees of freedom* of a *hp*-mesh $\mathscr{T}_{h\mathsf{p}}$ generated by $\mathcal{M}$ and $\mathcal{P}$ by

$$N(\mathcal{M},\mathcal{P}) := \int_\Omega \frac{d(x)}{\nu(x)}\,\mathrm{d}x = \int_\Omega \frac{2}{3\sqrt{3}}(\mathcal{P}(x)+1)(\mathcal{P}(x)+2)\left(\det\mathcal{M}(x)\right)^{1/2}\,\mathrm{d}x. \tag{2.23}$$

Hence, the function $\eta(x) := d(x)/\nu(x)$ represents the "density of the number of degrees of freedom".

3 The main problem formulation

In this section we formulate the main problem of this paper mentioned in Introduction. Namely, we introduce the criteria defining the optimal *hp*-grid for a given function $u:\Omega\to\mathbb{R}$. For simplicity, we deal with functions from $V := C^\infty(\Omega)$.

Let $u\in V$ be a given function, $\bar{x}\in\Omega$ and $p\in\mathbb{N}$ be an integer. We define the projection operator $\pi_{\bar{x},p}: V\to P^p(\bar{\Omega})$ such that

$$\frac{\partial^k}{\partial x_1^l\partial x_2^{k-l}}\pi_{\bar{x},p}u(\bar{x}) = \frac{\partial^k}{\partial x_1^l\partial x_2^{k-l}}u(\bar{x}) \quad \forall l=0,\dots,k \quad \forall k=0,\dots,p, \quad u\in V. \tag{3.1}$$

Therefore, $\pi_{\bar{x},p}u$ is the polynomial function of degree p on Ω which has the same values of all partial derivatives up to order p at $\bar{x}$ as the function u. The existence and uniqueness of $\pi_{\bar{x},p}u$ is obvious. Using the operator $\pi_{\bar{x},p}$, we define the projection into the space $S_{h\mathsf{p}}$.

Definition 3.1. Let $\mathscr{T}_{h\mathsf{p}} = (\mathscr{T}_h, \mathsf{p})$ be a *hp*-mesh, $x_K,\ K \in \mathscr{T}_h$ be the barycentres of $K \in \mathscr{T}_h$ and $S_{h\mathsf{p}}$ be the corresponding space of discontinuous piecewise polynomial functions defined by (2.2). We define the operator $\Pi_{h\mathsf{p}} : V \to S_{h\mathsf{p}}$ by

$$\Pi_{h\mathsf{p}} u|_K := \pi_{x_K, p_K} u|_K \quad \forall K \in \mathscr{T}_h. \tag{3.2}$$

Hence, the operator $\Pi_{h\mathsf{p}}$is defined separately for each $K \in \mathscr{T}_h$ and its definition is unique for the given *hp*-mesh.

Now, we are ready to formulate the main problem of this paper.

Problem 3.2. Let $u \in V$ be a given function, $q \in [1, \infty]$ be a given degree of the Lebesgue norm and $\omega > 0$ be a given tolerance. We *seek a hp-mesh* $\mathscr{T}_{h\mathsf{p}}$ such that

(P1) $\|u - \Pi_{h\mathsf{p}} u\|_{L^q(\Omega)} \le \omega$, where $\Pi_{h\mathsf{p}} : V \to S_{h\mathsf{p}}$ is defined by (3.2),

(P2) the number of degrees of freedom $N_{h\mathsf{p}}$ of $\mathscr{T}_{h\mathsf{p}}$ is minimal.

The Problem 3.2 is complex and we are not able to solve it. However, in virtue of Remark 2.10, we introduce two equivalent *auxiliary* local *problems* whose solution is an optimal anisotropic element with the barycentre at the given node $\bar{x} \in \Omega$. Then, using the solution of the auxiliary problem and heuristic considerations, we derive the Riemann metric $\mathcal{M} : \Omega \to \mathrm{Sym}$ and the polynomial degree distribution function $\mathcal{P} : \Omega \to \mathbb{R}^+$, which define the *hp*-mesh $\mathscr{T}_{h\mathsf{p}}$. This *hp*-mesh satisfies condition (P1) of Problem 3.2 and the corresponding number $N_{h\mathsf{p}}$ is small. Therefore, we expect that this resulting *hp*-mesh is close to the (hypothetical) solution of Problem 3.2.

3.1 Auxiliary problems

Let $u \in V$, $\bar{x} = (\bar{x}_1, \bar{x}_2) \in \Omega$ and $p \in \mathbb{N}$ be given. Using the Taylor expansion of degree $p+1$ at $\bar{x}$, we have

$$u(x) = \sum_{k=0}^{p+1} \frac{1}{k!} \left(\sum_{l=0}^{k} \binom{k}{l} \frac{\partial^k u(\bar{x})}{\partial x_1^l \partial x_2^{k-l}} (x_1 - \bar{x}_1)^l (x_2 - \bar{x}_2)^{k-l} \right) + O(|x - \bar{x}|^{p+2}),\ x \in \Omega, \tag{3.3}$$

where $\binom{k}{l} = \frac{k!}{l!(k-l)!}$. Let $\pi_{\bar{x},p} u$ be given by (3.1), then (3.3) reads

$$u(x) - \pi_{\bar{x},p} u(x) = e^{\mathrm{int}}_{\bar{x},p}(x) + O(|x - \bar{x}|^{p+2}), \tag{3.4}$$

where

$$e^{\mathrm{int}}_{\bar{x},p}(x) := \frac{1}{(p+1)!} \sum_{l=0}^{p+1} \left[\binom{p+1}{l} \frac{\partial^{p+1} u(\bar{x})}{\partial x_1^l \partial x_2^{p+1-l}} (x_1 - \bar{x}_1)^l (x_2 - \bar{x}_2)^{p+1-l} \right] \tag{3.5}$$

is the *interpolation error function* of degree p located at $\bar{x}$. Obviously, $e^{\mathrm{int}}_{\bar{x},p}(\bar{x}) = 0$ and $e^{\mathrm{int}}_{\bar{x},p}(x) \approx u(x) - \pi_{\bar{x},p} u(x)$ up to the higher order terms. Moreover, (3.2) and (3.4) give

$$(u - \Pi_{h\mathsf{p}} u)\,|_K \approx e^{\mathrm{int}}_{x_K, p_K}|_K \quad \forall K \in \mathscr{T}_h, \tag{3.6}$$

where x_K is the barycentre of $K \in \mathscr{T}_h$.

Now, we introduce the following auxiliary local problem.

Problem 3.3. Let $u \in V$, $\bar{x} \in \Omega$, $p \in \mathbb{N}$, $q \in [1, \infty]$ and $\bar{\omega} > 0$ be given. We seek an *anisotropic triangle* K (i.e., its anisotropy $\{h_K, \sigma_K, \phi_K\}$) having the barycentre at $\bar{x}$ such that

(p1) $\left\| e^{\mathrm{int}}_{\bar{x},p} \right\|_{L^q(K)} \le \bar{\omega}$,

(p2) the area of K is the maximal possible.

The condition (p2) follows from the consideration that in order to minimize the number N_{hp} of the *hp*-mesh, we have to construct triangles with the maximal possible area (for the given degree of the polynomial approximation).

We assume that Problem 3.3 is equivalent with the following one.

Problem 3.4. Let $u \in V$, $\bar{x} \in \Omega$, $p \in \mathbb{N}$ and $\bar{\nu} > 0$ be given. We seek an *anisotropic triangle* K with the barycentre at $\bar{x}$ such that

(p1*) $\left\|e^{\mathrm{int}}_{\bar{x},p}\right\|_{L^q(K)}$ is minimal,

(p2*) the area of K is equal to $\bar{\nu}$.

Remark 3.5. By the equivalency of Problems 3.3 and 3.4 we mean the following:

- If the triangle $\tilde{K}$ is the solution of Problem 3.3 then $\tilde{K}$ is also the solution Problem 3.4 with $\bar{\nu} := |\tilde{K}|$. Moreover, $\left\|e^{\mathrm{int}}_{\bar{x},p}\right\|_{L^q(\tilde{K})} = \bar{\omega}$.
- If the triangle $\tilde{K}$ is the solution of Problem 3.4 then $\tilde{K}$ is also the solution Problem 3.3 with $\bar{\omega} := \left\|e^{\mathrm{int}}_{\bar{x},p}\right\|_{L^q(\tilde{K})}$. Moreover, $|\tilde{K}| = \bar{\nu}$.

Let $B_1 := \{\xi;\ \xi = (\xi_1, \xi_2) \in \mathbb{R}^2,\ \xi_1^2 + \xi_2^2 = 1\}$ denote the unit sphere in $\mathbb{R}^2$. We define the k^{th}-(scaled) *directional derivative* of $u \in V$ along the direction $\xi \in B_1$ at $x \in \Omega$ by

$$\mathrm{d}^k u(x;\xi) := \frac{1}{k!} \sum_{l=0}^{k} \binom{k}{l} \frac{\partial^k u(x)}{\partial x_1^l \partial x_2^{k-l}}\, \xi_1^l\, \xi_2^{k-l}, \quad x \in \Omega,\ \xi = (\xi_1, \xi_2) \in B_1. \tag{3.7}$$

From (3.5) and (3.7), we deduce that

$$e^{\mathrm{int}}_{\bar{x},p}(x) = \mathrm{d}^{p+1} u\left(\bar{x}; \frac{x-\bar{x}}{|x-\bar{x}|}\right) |x-\bar{x}|^{p+1} \quad \forall x \in \Omega,\ p \in \mathbb{N},\ \bar{x} \in \Omega. \tag{3.8}$$

In order to understand the behaviour of $e^{\mathrm{int}}_{\bar{x},p}$, for the given $u \in V$, $\bar{x} \in \Omega$ and $p \in \mathbb{N}$, we define the domain

$$F^p := \{\bar{x}\} \cup \left\{ x \in \mathbb{R}^2;\ x \neq \bar{x},\ |x-\bar{x}| \leq \left| \mathrm{d}^{p+1} u\left(\bar{x}; \frac{x-\bar{x}}{|x-\bar{x}|}\right)\right| = \frac{\left|e^{\mathrm{int}}_{\bar{x},p}(x)\right|}{|x-\bar{x}|^{p+1}} \right\}. \tag{3.9}$$

The geometric meaning of F^p is the following. If $x \in F^p$ then its distance to $\bar{x}$ is less or equal to the directional derivative $\mathrm{d}^{p+1}u(\bar{x},\cdot)$ along the direction $(x-\bar{x})/|x-\bar{x}|$. In the other words, F^p is the image of a unit ball with the center at $\bar{x}$ given by the mapping $\zeta \to \mathrm{d}^{p+1}u(\bar{x};\zeta/|\zeta|)\zeta$. Hence, it shows the size of the scaled directional derivative of $u \in V$ at $\bar{x} \in \Omega$ along each direction $\xi \in B_1$.

Example 3.6. Let us consider the function

$$u(x_1, x_2) = 0.01(6x_1^7 + 4x_1^6 x_2 - 3x_1^5 x_2^2 + 8x_1^4 x_2^3 + 12x_1^3 x_2^4 + 5x_1^2 x_2^5 + x_1 x_2^6 - x_2^7). \tag{3.10}$$

Figure 2 shows the sets F^p for $p = 1, 3, 5$, $\bar{x} = (1,1)$ and u given by (3.10).

3.2 Anisotropy of the interpolation error function

The interpolation error function $e^{\mathrm{int}}_{\bar{x},p}$ depends in general on all partial derivatives of order $p+1$ of u. In order to solve Problems 3.3 and 3.4, it is advantageous to estimate $e^{\mathrm{int}}_{\bar{x},p}$ by an expression depending on three parameters only since the anisotropy of a triangle is given by 3 parameters: its size, aspect ratio and orientation.

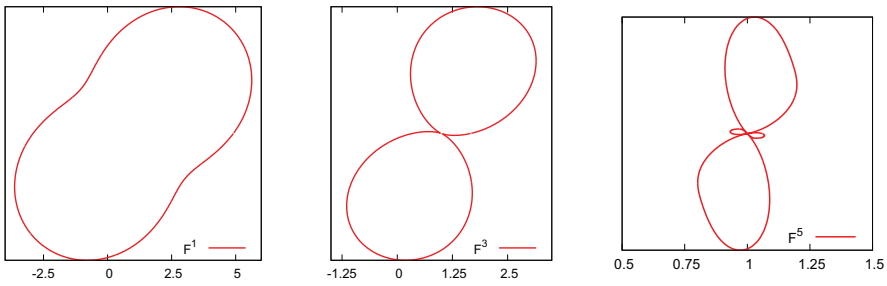

Fig. 2: The boundaries of domains F^p, $p = 1, 3, 5$ for Example 3.6.

First, we consider the case $p = 1$. Let $\bar{x} \in \Omega$, $u \in V$ and $p = 1$ be given. We define the values $A_1 \geq 0$, $\xi_1 \in B_1$, $\varphi_1 \in [0, 2\pi)$, $A_1^\perp \geq 0$, $\xi_1^\perp \in B_1$ and $\rho_1 \geq 1$ by

$$A_1 := \max_{\xi \in B_1} |\mathrm{d}^2 u(\bar{x}; \xi)|, \tag{3.11a}$$

$$\xi_1 := \arg\max_{\xi \in B_1} |\mathrm{d}^2 u(\bar{x}; \xi)|, \tag{3.11b}$$

$$\varphi_1 \in [0, 2\pi) \text{ such that } (\cos\varphi_1, \sin\varphi_1)^{\mathrm{T}} = \xi_1, \tag{3.11c}$$

$$A_1^\perp := |\mathrm{d}^2 u(\bar{x}; \xi_1^\perp)|, \text{ where } \xi_1^\perp \in B_1,\ \xi_1^\perp \cdot \xi_1 = 0, \tag{3.11d}$$

$$\rho_1 := \frac{A_1}{A_1^\perp}, \tag{3.11e}$$

where $a \cdot b = (a_1 b_1 + a_2 b_2)$, $a, b \in \mathbb{R}^2$ is the scalar product in $\mathbb{R}^2$. It means that A_1 is the maximal value of the second order scaled directional derivative of u at $\bar{x}$, ξ_1 is the direction which maximizes this derivative, φ_1 is the angle corresponding to ξ_1, $\xi_1^\perp$ is the direction perpendicular to ξ_1, $A_1^\perp$ is the second order scaled directional derivative of u along the direction $\xi_1^\perp$ at $\bar{x}$ and ρ_1 is the ratio between A_1 and $A_1^\perp$.

Let us define a matrix $\mathbb{D}_{\rho_1}$ by

$$\mathbb{D}_{\rho_1} := \begin{pmatrix} 1 & 0 \\ 0 & (\rho_1)^{-1} \end{pmatrix}, \tag{3.12}$$

where ρ_1 is given by (3.11e). Then, we have the following equality.

Lemma 3.7. *Let $\bar{x} \in \Omega$, $u \in V$ and $p = 1$ be given. We set $A_1 \geq 0$, $\varphi_1 \in [0, 2\pi)$ and ρ_1 by* (3.11a), (3.11c) *and* (3.11e), *respectively. Then*

$$\left|e^{\mathrm{int}}_{\bar{x},1}(x)\right| = \left|e^{\mathrm{int}}_{\bar{x},1}(\bar{x} + \zeta)\right| = A_1 \zeta^{\mathrm{T}} \mathbb{Q}_{\varphi_1} \mathbb{D}_{\rho_1} \mathbb{Q}_{\varphi_1}^{\mathrm{T}} \zeta \quad \forall \zeta = x - \bar{x},\ x \in \Omega, \tag{3.13}$$

where $e^{\mathrm{int}}_{\bar{x},1}$ is given by (3.5), *$\mathbb{Q}_{\varphi_1}$ is the rotation* (2.6) *and $\mathbb{D}_{\rho_1}$ is defined by* (3.12).

Proof. Obviously, both sides of (3.13) are 2-homogeneous with respect to ζ, i.e.,

$$\begin{aligned} e^{\mathrm{int}}_{\bar{x},1}(\bar{x} + \beta\zeta) &= \beta^2 e^{\mathrm{int}}_{\bar{x},1}(\bar{x} + \zeta) && \forall \zeta \in \mathbb{R}^2\, \forall \beta \in \mathbb{R}, \\ A_1 (\beta\zeta)^{\mathrm{T}} \mathbb{Q}_{\varphi_1} \mathbb{D}_{\rho_1} \mathbb{Q}_{\varphi_1}^{\mathrm{T}} (\beta\zeta) &= \beta^2\, A_1 \zeta^{\mathrm{T}} \mathbb{Q}_{\varphi_1} \mathbb{D}_{\rho_1} \mathbb{Q}_{\varphi_1}^{\mathrm{T}} \zeta && \forall \zeta \in \mathbb{R}^2\, \forall \beta \in \mathbb{R}. \end{aligned} \tag{3.14}$$

Therefore, it is enough to prove (3.13) for all $\zeta \in B_1$, where B_1 is the unit sphere in $\mathbb{R}^2$. From (3.5), we have

$$e^{\mathrm{int}}_{\bar{x},1}(\bar{x} + \zeta) = \frac{1}{2} \sum_{i,j=1}^{2} \frac{\partial^2 u(\bar{x})}{\partial x_i \partial x_j} \zeta_i \zeta_j = \frac{1}{2} \zeta^{\mathrm{T}} \mathbb{H} \zeta \quad \forall \zeta = (\zeta_1, \zeta_2), \quad \mathbb{H} := \left\{ \frac{\partial^2 u(\bar{x})}{\partial x_i \partial x_j} \right\}_{i,j=1}^{2}, \tag{3.15}$$

where $\mathbb{H}$ is the Hessian matrix. Since $\mathbb{H}$ is symmetric, we decompose it in the form

$$\mathbb{H} = \mathbb{Q}_\phi^{\mathrm{T}} \mathrm{diag}(\lambda_1, \lambda_2) \mathbb{Q}_\phi = \mathbb{Q}_\phi^{\mathrm{T}} \begin{pmatrix} \lambda_1 & 0 \\ 0 & \lambda_2 \end{pmatrix} \mathbb{Q}_\phi, \tag{3.16}$$

where λ_1, λ_2 are the real eigenvalues of $\mathbb{H}$ and $\mathbb{Q}_\phi$ is the rotation through angle $\phi \in [0, 2\pi)$ given by (2.6). The eigenvalues are indexed such that $|\lambda_1| \geq |\lambda_2|$. The columns of $\mathbb{Q}_\phi$ are the eigenvectors corresponding to λ_1 and λ_2, hence the eigenvector corresponding to λ_1 is $(\cos\phi, \sin\phi)^{\mathrm{T}}$.

Moreover, we express $\zeta \in B_1$ as a function of the corresponding angle, i.e., $\zeta = \zeta(\alpha) = (\cos\alpha, \sin\alpha)^{\mathrm{T}}$, $\alpha \in [0, 2\pi)$. By a direct computation, we have $\mathbb{Q}_\phi \zeta = (\cos(\phi+\alpha), \sin(\phi+\alpha))^{\mathrm{T}}$. Then, using (3.15) – (3.16), we obtain

$$\begin{aligned} e^{\mathrm{int}}_{\bar{x},1}(\bar{x}+\zeta) &= \frac{1}{2}\zeta^{\mathrm{T}} \mathbb{H} \zeta = \frac{1}{2}\zeta^{\mathrm{T}} \mathbb{Q}_\phi^{\mathrm{T}} \mathrm{diag}(\lambda_1, \lambda_2) \mathbb{Q}_\phi \zeta \\ &= \frac{1}{2}(\cos(\phi+\alpha), \sin(\phi+\alpha)) \begin{pmatrix} \lambda_1 & 0 \\ 0 & \lambda_2 \end{pmatrix} \begin{pmatrix} \cos(\phi+\alpha) \\ \sin(\phi+\alpha) \end{pmatrix}. \end{aligned} \tag{3.17}$$

On the other hand, $\mathbb{Q}_{\varphi_1}^{\mathrm{T}} \zeta = (\cos(\alpha-\varphi_1), \sin(\alpha-\varphi_1))^{\mathrm{T}}$ and the right-hand side of (3.13) can be expressed by

$$A_1 \zeta^{\mathrm{T}} \mathbb{Q}_{\varphi_1} \mathbb{D}_{\rho_1} \mathbb{Q}_{\varphi_1}^{\mathrm{T}} \zeta = (\cos(\alpha-\varphi_1), \sin(\alpha-\varphi_1)) \begin{pmatrix} A_1 & 0 \\ 0 & A_1/\rho_1 \end{pmatrix} \begin{pmatrix} \cos(\alpha-\varphi_1) \\ \sin(\alpha-\varphi_1) \end{pmatrix}. \tag{3.18}$$

Therefore, (3.17) and (3.18) implies that in order to prove (3.13), we have to show that $A_1 = \lambda_1/2$, $A_1/\rho_1 = \lambda_2/2$ and $\phi = -\varphi_1$. The relation (3.17) implies that

$$|e^{\mathrm{int}}_{\bar{x},1}(x)| = |e^{\mathrm{int}}_{\bar{x},1}(\bar{x}+\zeta(\alpha))| = \frac{1}{2}\left|\lambda_1 \cos^2(\phi+\alpha) + \lambda_2 \sin^2(\phi+\alpha)\right|, \quad \alpha \in [0, 2\pi). \tag{3.19}$$

Since $|\lambda_1| \geq \lambda_2$, then

$$\max_{\alpha\in[0,2\pi)} |e^{\mathrm{int}}_{\bar{x},1}(\bar{x}+\zeta(\alpha))| = \frac{|\lambda_1|}{2}, \quad \arg\max_{\alpha\in(0,2\pi)} |e^{\mathrm{int}}_{\bar{x},1}(\bar{x}+\zeta(\alpha))| = -\phi, \tag{3.20}$$

which together with (3.8) and (3.11a)–(3.11c) gives

$$\begin{aligned} A_1 &= \max_{\xi\in B_1} |\mathrm{d}^2 u(\bar{x};\xi)| = \max_{\alpha\in[0,2\pi)} |e^{\mathrm{int}}_{\bar{x},1}(\bar{x}+\zeta(\alpha))| = \frac{|\lambda_1|}{2}, \\ \xi_1 &= \arg\max_{\xi\in B_1} |\mathrm{d}^2 u(\bar{x};\xi)| = \arg\max_{\alpha\in(0,2\pi)} |e^{\mathrm{int}}_{\bar{x},1}(\bar{x}+\zeta(\alpha))| = -\phi. \end{aligned} \tag{3.21}$$

Moreover, let $\phi^\perp := -\phi + \pi/2$ then the vector $(\cos\phi^\perp, \sin\phi^\perp)$ is perpendicular to the vector $(\cos(-\phi), \sin(-\phi))$. The relation (3.19) implies

$$|e^{\mathrm{int}}_{\bar{x},1}(\bar{x}+\zeta(\phi^\perp))| = \frac{|\lambda_2|}{2}. \tag{3.22}$$

Using (3.8), (3.11d)–(3.11e) and (3.22), we obtain

$$A_1/\rho_1 = A_1^\perp = |\mathrm{d}^2 u(\bar{x};\xi_1^\perp)| = |e^{\mathrm{int}}_{\bar{x},1}(\bar{x}+\zeta(\phi^\perp))| = \frac{|\lambda_2|}{2}, \tag{3.23}$$

which together with (3.17), (3.18) and (3.21) proves (3.13). □

The relation (3.13) represents the estimate of the interpolation error function $e^{\mathrm{int}}_{\bar{x},p}$ for $p = 1$ using the quantities A_1, ρ_1 and φ_1 denoting the size, the aspect ratio and the orientation of the interpolation error function, respectively.

Our aim is to find an estimate of $e^{\mathrm{int}}_{\bar{x},p}$ also for $p > 1$. Motivated by [6, 7], we intent to derive the *anisotropic estimate* in the form

$$\left|e^{\mathrm{int}}_{\bar{x},p}(x)\right| = \left|\mathrm{d}^{p+1}u\left(\bar{x}; \frac{\zeta}{|\zeta|}\right)|\zeta|^{p+1}\right| \leq A_p\left(\zeta^{\mathrm{T}}\mathbb{Q}_{\varphi_p}\mathbb{D}_{\rho_p}\mathbb{Q}^{\mathrm{T}}_{\varphi_p}\zeta\right)^{\frac{p+1}{2}} \quad \forall \zeta = x - \bar{x},\ x \in \Omega, \tag{3.24}$$

where $\mathbb{Q}_{\varphi_p}$ is the rotation through angle φ_p (2.6) and $\mathbb{D}_{\rho_p}$ is the matrix given by

$$\mathbb{D}_\rho := \begin{pmatrix} 1 & 0 \\ 0 & \rho^{-\frac{2}{p+1}} \end{pmatrix}, \quad \rho \geq 1, \tag{3.25}$$

the parameter ρ plays a role of the anisotropy. The values $A_p \geq 0$, $\rho_p \geq 1$ and $\varphi_p \in [0, 2\pi)$ represent the size, the aspect ratio and the orientation of the interpolation error function $e^{\mathrm{int}}_{\bar{x},p}$, which have to be defined.

First, we formally extend (3.11) for $p > 1$. Let $\bar{x} \in \Omega$, $u \in V$ and $p \in \mathbb{N}$ be given. We define the values $\tilde{A}_p \geq 0$, $\tilde{\xi}_p \in B_1$, $\tilde{\varphi}_p \in [0, 2\pi)$, $\tilde{A}^{\perp}_p \geq 0$ and $\tilde{\rho}_p \geq 1$ by

$$\tilde{A}_p := \max_{\xi \in B_1} |\mathrm{d}^{p+1}u(\bar{x}; \xi)|, \tag{3.26a}$$

$$\tilde{\xi}_p := \arg\max_{\xi \in B_1} |\mathrm{d}^{p+1}u(\bar{x}; \xi)|, \tag{3.26b}$$

$$\tilde{\varphi}_p \in [0, 2\pi) \text{ such that } (\cos\tilde{\varphi}_p, \sin\tilde{\varphi}_p)^{\mathrm{T}} = \tilde{\xi}_p, \tag{3.26c}$$

$$\tilde{A}^{\perp}_p := |\mathrm{d}^{p+1}u(\bar{x}; \tilde{\xi}^{\perp}_p)|, \text{ where } \xi^{\perp}_p \in B_1,\ \tilde{\xi}^{\perp}_p \cdot \tilde{\xi}_p = 0, \tag{3.26d}$$

$$\tilde{\rho}_p := \frac{\tilde{A}_p}{\tilde{A}^{\perp}_p}. \tag{3.26e}$$

Hence, $\tilde{A}_p$ is the maximal value of the $(p+1)^{\mathrm{th}}$-order scaled directional derivative of u at $\bar{x}$, $\tilde{\xi}_p$ is the direction which maximizes this derivative, $\tilde{\varphi}_p$ is the angle corresponding to $\tilde{\xi}_p$, $\tilde{A}^{\perp}_p$ is the $(p+1)^{\mathrm{th}}$-order scaled directional derivative of u along the direction perpendicular to $\tilde{\xi}_p$ and $\tilde{\rho}_p$ is the ratio between $\tilde{A}_p$ and $\tilde{A}^{\perp}_p$.

However, numerical experiments show (see Example 3.8) that the estimate

$$\left|e^{\mathrm{int}}_{\bar{x},p}(\bar{x} + \zeta)\right| \leq \tilde{A}_p\left(\zeta^{\mathrm{T}}\mathbb{Q}_{\tilde{\varphi}_p}\mathbb{D}_{\tilde{\rho}_p}\mathbb{Q}^{\mathrm{T}}_{\tilde{\varphi}_p}\zeta\right)^{\frac{p+1}{2}}, \quad \zeta \in \mathbb{R}^2 \tag{3.27}$$

does not valid for the values $\tilde{A}_p$, $\tilde{\varphi}_p$ and $\tilde{\rho}_p$ defined by (3.26a), (3.26c) and (3.26e), respectively

Example 3.8. Let $\bar{x} \in \Omega$, $p \in \mathbb{N}$, $A \geq 0$, $\rho \geq 1$ and $\varphi \in [0, 2\pi)$ be given. We define the domain

$$\mathscr{G}(p, A, \rho, \varphi) := \{\bar{x}\} \cup \left\{ \bar{x} + \zeta \in \mathbb{R}^2;\ \zeta \neq 0,\ |\zeta| \leq \frac{A\left(\zeta^{\mathrm{T}}\mathbb{Q}_{\varphi}\mathbb{D}_{\rho}\mathbb{Q}^{\mathrm{T}}_{\varphi}\zeta\right)^{\frac{p+1}{2}}}{|\zeta|^{p+1}} \right\}. \tag{3.28}$$

We consider again the function u given by (3.10), $\bar{x} = (1, 1)$ and $p = 1, 3, 5$. Figure 3 shows the domains F^p, $p = 1, 3, 5$ (given by (3.9)) and the domains $G^p = \mathscr{G}(p, \tilde{A}_p, \tilde{\rho}_p, \tilde{\varphi}_p)$, $p = 1, 3, 5$, where $\tilde{A}_p$, $\tilde{\varphi}_p$ and $\tilde{\rho}_p$ are given by (3.26a), (3.26c) and (3.26e), respectively. We observe that $F^p \not\subset G^p$ for some p, which means that the inequality (3.27) does not valid in general, compare (3.9) with (3.28).

Remark 3.9. Let us note that the domain $\mathscr{G}(p, A, \rho, \varphi)$ can be parametrized in the coordinate system $(\tilde{x}_1, \tilde{x}_2)$, where $\tilde{x}_1$ is parallel with the direction $(\cos\varphi, \sin\varphi)^{\mathrm{T}}$ by

$$\left.\begin{aligned} \tilde{x}_1 &= t\cos\phi\left(A^{\frac{1}{p+1}}\cos^2\phi + (A/\rho)^{\frac{1}{p+1}}\sin^2\phi\right)^{p+1} \\ \tilde{x}_2 &= t\sin\phi\left(A^{\frac{1}{p+1}}\cos^2\phi + (A/\rho)^{\frac{1}{p+1}}\sin^2\phi\right)^{p+1} \end{aligned}\right\} \quad \begin{aligned} &t \in [0, 1], \\ &\phi \in [0, 2\pi). \end{aligned} \tag{3.29}$$

Obviously, if $\rho = 1$ then $\mathscr{G}$ reduce to the circle with the radius A.

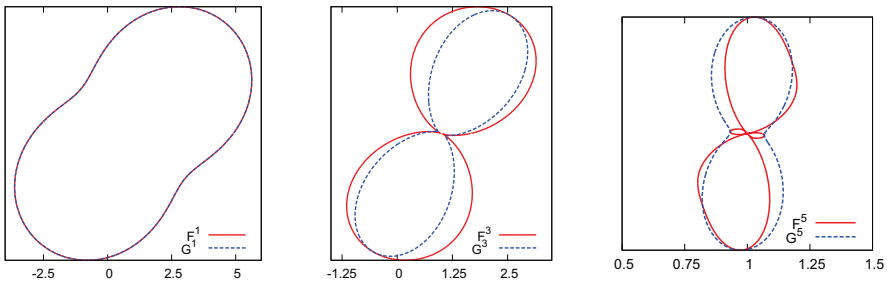

Fig. 3: The boundaries of domains F^p, $G^p = \mathscr{G}(p, \tilde{A}_p, \tilde{\rho}_p, \tilde{\varphi}_p)$ for Example 3.8.

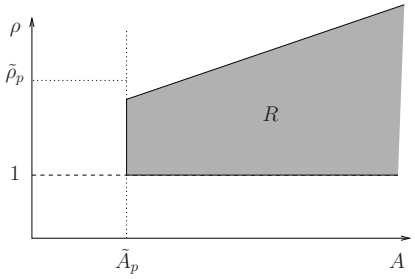

Fig. 4: Example of the set R given by (3.32), the values $\tilde{A}_p$ and $\tilde{\rho}_p$ are given by (3.26a) and (3.26e), respectively.

Probably, the estimate (3.27) is valid with some constant $C > 0$, i.e.,

$$\left|e^{\mathrm{int}}_{\bar{x},p}(x)\right| \le C\tilde{A}_p \left(\zeta^{\mathrm{T}}\mathbb{Q}_{\tilde{\varphi}_p}\mathbb{D}_{\tilde{\rho}_p}\mathbb{Q}^{\mathrm{T}}_{\tilde{\varphi}_p}\zeta\right)^{\frac{p+1}{2}} \qquad \forall \zeta = x - \bar{x},\ x \in \Omega, \tag{3.30}$$

however, we are not able to verify it. Therefore, we modify the definitions of $\tilde{A}_p$ and $\tilde{\rho}_p$ such that the estimate (3.24) will be valid without any unknown constant.

Let $\bar{x} \in \Omega$, $u \in V$ and $p \in \mathbb{N}$ be given. Similarly as in (3.26b) – (3.26c), we put

$$\xi_p := \arg\max_{\xi \in B_1} |\mathrm{d}^{p+1}u(\bar{x};\xi)|, \tag{3.31a}$$

$$\varphi_p \in [0, 2\pi) \text{ such that } (\cos\varphi_p, \sin\varphi_p)^{\mathrm{T}} = \xi_p, \tag{3.31b}$$

hence the $(p+1)^{\mathrm{th}}$-order scaled directional derivative of u at $\bar{x}$ is the maximal along the direction $(\cos\varphi_p, \sin\varphi_p)$. We define the set of pairs (A, ρ) by

$$R := \left\{(A,\rho);\ A \ge 0,\ \rho \ge 1 : \left|e^{\mathrm{int}}_{\bar{x},p}(\bar{x}+\zeta)\right| \le A\left(\zeta^{\mathrm{T}}\mathbb{Q}_{\varphi_p}\mathbb{D}_{\rho}\mathbb{Q}^{\mathrm{T}}_{\varphi_p}\zeta\right)^{\frac{p+1}{2}}\ \ \forall \zeta \in \mathbb{R}^2\right\}. \tag{3.32}$$

Obviously, $R \subset \mathbb{R}^2$ is nonempty since $(\tilde{A}_p, 1) \in R$, where $\tilde{A}_p$ is given by (3.26a). This follows from (3.7), (3.8), (3.26a) and the fact that $\zeta^{\mathrm{T}}\mathbb{Q}_{\varphi_p}\mathbb{D}_{\rho}\mathbb{Q}^{\mathrm{T}}_{\varphi_p}\zeta = |\zeta|^2$ for $\rho = 1$. Moreover, if a pair $(A, \rho) \in R$ then $(A', \rho') \in R$ for any $A' \ge A$ and $\rho' \in [1, \rho]$. On the other hand, if $A' < \tilde{A}_p$ and $\rho' > \tilde{\rho}_p$, where $\tilde{A}_p$ and $\tilde{\rho}_p$ are given by (3.26a) and (3.26e), respectively, then $(A', \rho') \notin R$. An example of the set R is shown in Figure 4.

Obviously, if we choose any pair (A_p, ρ_p) from R and φ_p is given by (3.31b), then the estimate (3.24) is valid and the corresponding set $\mathscr{G}(p, A_p, \rho_p, \varphi_p)$, given by (3.28), satisfies $F^p \subset \mathscr{G}(p, \tilde{A}_p, \tilde{\rho}_p, \tilde{\varphi}_p)$. On the other hand, in order not to "over-estimate" $e^{\mathrm{int}}_{\bar{x},p}$, it is desirable to choose

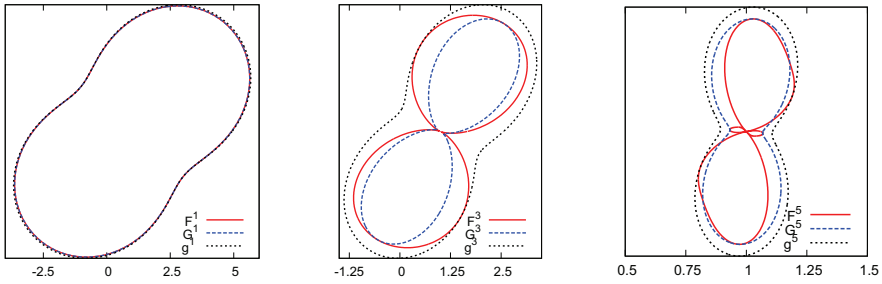

Fig. 5: The boundaries of domains F^p, $G^p = \mathscr{G}(p, \tilde{A}_p, \tilde{\rho}_p, \tilde{\varphi}_p)$ and $g^p = \mathscr{G}(p, A_p, \rho_p, \varphi_p)$ for Example 3.8.

the pair (A_p, ρ_p) from R such that the corresponding set $\mathscr{G}(p, A_p, \rho_p, \varphi_p)$ has the minimal possible area. Therefore we define the values A_p, ρ_p and φ_p (already defined by (3.31b)) by

$$\varphi_p \in [0, 2\pi) \text{ such that } (\cos\varphi_p, \sin\varphi_p)^{\mathrm{T}} = \arg\max_{\xi\in B_1} |\mathrm{d}^{p+1}u(\bar{x};\xi)| \tag{3.33}$$
$$(A_p, \rho_p) := \arg\min_{A,\rho\in R} |\mathscr{G}(p, A, \rho, \varphi_p)|$$

where R and $\mathscr{G}$ are given by (3.32) and (3.28), respectively, and $|\mathscr{G}(p, A, \rho, \varphi_p)|$ denotes the area of $\mathscr{G}(p, A, \rho, \varphi_p)$. Using the parametrization (3.29), we derive

$$|\mathscr{G}(p, A, \rho, \phi| = \int_{t=0}^{1}\int_{\phi=0}^{2\pi} \det\frac{D(\tilde{x}_1, \tilde{x}_2)}{D(t, \phi)}\mathrm{d}\phi\,\mathrm{d}t = A^2 \sum_{l=0}^{2(p+1)} c_l \rho^{-\frac{l}{p+1}}, \tag{3.34}$$

where

$$c_l = 2\binom{2(p+1)}{l}\int_0^{\pi/2}(\sin\phi)^{2l}(\cos\phi)^{2(p+1-l)}\mathrm{d}\phi, \quad l = 0, \ldots, 2(p+1). \tag{3.35}$$

The coefficients c_l, $l = 0, \ldots, 2(p+1)$ can be expressed analytically. Figure 5 shows the domain F^p (given by (3.9)), the domain $G^p = \mathscr{G}(p, \tilde{A}_p, \tilde{\rho}_p, \varphi_p)$ with the parameters $\tilde{A}_p$, $\tilde{\varphi}_p$ and $\tilde{\rho}_p$ defined by (3.26a), (3.26c) and (3.26e), respectively, and the domain $g^p := \mathscr{G}(p, A_p, \rho_p, \varphi_p)$ with the optimal parameters A_p, φ_p and ρ_p defined by (3.33) for $p = 1, 3, 5$. We observe that $F^p \subset g^p$ for each p. Moreover, the estimate (3.24), which is valid, is not over-estimated, since the boundary of F^p touch the boundary of g^p from the interior.

Remark 3.10. The values A_p, ρ_p and φ_p given by (3.33) can by evaluated approximately by the following iterative algorithm. First, we find φ_p by seeking the maximum of $|\mathrm{d}^{p+1}u(\bar{x};\xi)|$ over the set $\xi \in \Xi := \{\cos(i\pi/n), \sin(i\pi/n),\ i = 1, \ldots, n\}$, where n is a suitable chosen parameter. E.g., the choice $n = 180$ gives the angle φ_p with the accuracy $1°$. Secondly, we put $A_p^{(l)} := \tilde{A}_p\gamma^l$, $l = 0, 1, \ldots$, where $\tilde{A}_p$ is given by (3.26a) and $\gamma > 1$ is a chosen constant. For each $l = 0, 1, \ldots$, we find the maximal value $\rho_p^{(l)} \geq 1$ such that $F^p \subset \mathscr{G}(p, A_p^{(l)}, \rho_p^{(l)}, \varphi_p) \Longleftrightarrow$ (3.24) is valid. The value $\rho_p^{(l)}$ always exists since $F^p \subset \mathscr{G}(p, A, 1, \varphi_p)$ for any $A \geq \tilde{A}_p$. Again, it is sufficient to test (3.24) for $\zeta \in \Xi$. The relation (3.34) implies that the area of $\mathscr{G}$ depends monotonously on A and ρ. Hence, we proceed with the iterations $l = 0, 1, \ldots$ until the area of $\mathscr{G}(p, A_p^{(l)}, \rho_p^{(l)}, \varphi_p)$ decreases otherwise we stop the iterative process. Let us note, that this algorithm is not time consuming in comparison to the anisotropic mesh adaptation.

A simple consequence of (3.32) and (3.33) is the following *anisotropic estimate* of the interpolation error function.

Lemma 3.11. *Let $\bar{x} \in \Omega$, $u \in V$ and $p \in \mathbb{N}$ be given. Let $A_p \geq 0$, ρ_p and $\varphi_p \in [0, 2\pi)$ be given by* (3.33)*. Then*

$$\left|e^{\mathrm{int}}_{\bar{x},p}(x)\right| \leq A_p \left((x-\bar{x})^{\mathrm{T}} \mathbb{Q}_{\varphi_p} \mathbb{D}_{\rho_p} \mathbb{Q}^{\mathrm{T}}_{\varphi_p} (x-\bar{x})\right)^{\frac{p+1}{2}} \quad \forall x \in \Omega, \tag{3.36}$$

where $\mathbb{Q}_{\varphi_p}$ is the rotation (2.6)*, and $\mathbb{D}_{\rho_p}$ is defined by* (3.25)*. Moreover, the estimate* (3.36) *is sharp, i.e., there exists $x \in \Omega$ such that*

$$\left|e^{\mathrm{int}}_{\bar{x},p}(x)\right| = A_p \left((x-\bar{x})^{\mathrm{T}} \mathbb{Q}_{\varphi_p} \mathbb{D}_{\rho_p} \mathbb{Q}^{\mathrm{T}}_{\varphi_p} (x-\bar{x})\right)^{\frac{p+1}{2}}.$$

Now, we define the anisotropy of the interpolation error function $e^{\mathrm{int}}_{\bar{x},p}$.

Definition 3.12. Let $\bar{x} \in \Omega$, $u \in V$ and $p \in \mathbb{N}$ be given. The triple $\{A_p, \varphi_p, \rho_p\}$ defined by (3.33) is called the *anisotropy* of the interpolation error function $e^{\mathrm{int}}_{\bar{x},p}$.

Let us note that the defined anisotropy of $e^{\mathrm{int}}_{\bar{x},p}$ differs from the anisotropy presented in [6, 7]. The importance of estimate (3.36) is the following: whereas the interpolation error function (as well as F^p) depends on all partial derivatives of order $p+1$, the right-hand side of (3.36) (as well as $g^p = \mathscr{G}(p, A_p, \rho_p, \varphi_p)$) depends only on three parameters A_p, φ_p and ρ_p for fixed p. Moreover, estimate (3.36) is independent of a generic constant.

3.3 Solution of the auxiliary Problems 3.3 and 3.4

In order to solve the auxiliary Problem 3.4, we have to evaluate $\left\|e^{\mathrm{int}}_{\bar{x},p}\right\|_{L^q(K)}$, which requires a (little complicated) integration over a triangle K. We simplify this task by a modification of Problem 3.4 in such a way that we replace the sought triangle K by its corresponding ellipse E, see Definition 2.2. Since $K \subset E$ then we have the bound $\left\|e^{\mathrm{int}}_{\bar{x},p}\right\|_{L^q(K)} \leq \left\|e^{\mathrm{int}}_{\bar{x},p}\right\|_{L^q(E)}$.

Hence, let $\bar{x} \in \Omega$, $u \in V$, $p \in \mathbb{N}$ be given and let $\{A_p, \varphi_p, \rho_p\}$ be the anisotropy of the corresponding interpolation error function $e^{\mathrm{int}}_{\bar{x},p}$ introduced in Definition 3.12. We seek an ellipse E having barycentre $\bar{x}$ with the anisotropy $\{h_E, \sigma_E, \phi_E\}$ (introduced by Definition 2.3) such that

(p2**) the area of E is equal to the given value $\nu_{\bar{x},p} > 0$,

(p1**) $\left\|e^{\mathrm{int}}_{\bar{x},p}\right\|_{L^q(E)}$ is minimal.

We denote by h_E and $h^{\perp}_E = h_E/\sigma_E$ the size of the semi-axes of the sought ellipse E and the angle between the main axes of E and axis x_1 by ϕ_E. Let $\hat{E} := \{\xi \in \mathbb{R}^2;\ |\xi| \leq 1\}$ be the closed unit ball (= the reference circle), we define the mapping $\boldsymbol{F}_E : \hat{E} \to \mathbb{R}^2$ by

$$\boldsymbol{F}_E(\hat{x}) := \mathbb{Q}_{\phi_E} \mathbb{S}_E \hat{x} + \bar{x}, \tag{3.37}$$

where $\mathbb{Q}_{\phi_E}$ is the rotation trough angle ϕ_E given by (2.6) and

$$\mathbb{S}_E = \begin{pmatrix} h_E & 0 \\ 0 & h^{\perp}_E \end{pmatrix} = h_E \begin{pmatrix} 1 & 0 \\ 0 & \frac{1}{\sigma_E} \end{pmatrix}. \tag{3.38}$$

We can simply verify that $\boldsymbol{F}_E$ maps $\hat{E}$ onto E, i.e., $\boldsymbol{F}_E(\hat{E}) = E$. Moreover, let us note that if $\hat{K}$ is the reference equilateral triangle having vertices $[1;0]$, $[-\frac{1}{2}, \frac{\sqrt{3}}{2}]$ and $[-\frac{1}{2}, -\frac{\sqrt{3}}{2}]$ (lying on $\partial\hat{E}$) then its image $K = \boldsymbol{F}_E(\hat{K})$ is the isosceles triangle with the anisotropy $\{h_E, \sigma_E, \phi_E\}$ and the barycentre at $\bar{x}$. In virtue of Definition 2.2, this ellipse E (and the triangle K) are generated by the matrix

$$\mathbb{M}_{\bar{x},p} := \mathbb{Q}^{\mathrm{T}}_{\phi_E} \begin{pmatrix} \frac{1}{h_E^2} & 0 \\ 0 & \frac{1}{(h^{\perp}_E)^2} \end{pmatrix} \mathbb{Q}_{\phi_E} = \frac{1}{h_E^2} \mathbb{Q}^{\mathrm{T}}_{\phi_E} \begin{pmatrix} 1 & 0 \\ 0 & \sigma_E^2 \end{pmatrix} \mathbb{Q}_{\phi_E}. \tag{3.39}$$

Furthermore, (3.37) implies that

$$x = \boldsymbol{F}_E(\hat{x}) \quad \Rightarrow \quad x - \bar{x} = \mathbb{Q}_{\phi_E} \mathbb{S}_E \hat{x} \quad \Rightarrow \quad (x-\bar{x})^{\mathrm{T}} = \hat{x}^{\mathrm{T}} \mathbb{S}^{\mathrm{T}}_E \mathbb{Q}^{\mathrm{T}}_{\phi_E}. \tag{3.40}$$

Finally, the Jacobi matrix $\frac{D\boldsymbol{F}_E}{D\hat{x}} = \mathbb{Q}_{\phi_E}\mathbb{S}_E$ has the determinant $\det \frac{D\boldsymbol{F}_E}{D\hat{x}} = h_E h_E^{\perp}$. The area of the ellipse E is equal to

$$\nu_{\bar{x},p} = \pi h_E h_E^{\perp} = \pi h_E^2/\sigma_E = \pi \det \mathbb{S}_E. \tag{3.41}$$

In the following, we derive the optimal orientation ϕ_E and the aspect ratio σ_E of E in the L^q-norm, $1 \le q < \infty$ and in the L^∞-norm separately.

3.3.1 Estimate in the L^q-norm, $1 \le q < \infty$

With the aid of (3.36), the theorem of substitution and (3.40), we have

$$\begin{aligned}\left\|e^{\mathrm{int}}_{\bar{x},p}\right\|^q_{L^q(E)} &= \int_E \left|e^{\mathrm{int}}_{\bar{x},p}(x)\right|^q \,\mathrm{d}x \le \int_E A_p^q \left((x-\bar{x})^{\mathrm{T}}\mathbb{Q}_{\varphi_p}\mathbb{D}_{\rho_p}\mathbb{Q}^{\mathrm{T}}_{\varphi_p}(x-\bar{x})\right)^{\frac{q(p+1)}{2}} \,\mathrm{d}x \\ &= \int_{\hat{E}} A_p^q \left(\hat{x}^{\mathrm{T}}\mathbb{S}_E^{\mathrm{T}}\mathbb{Q}^{\mathrm{T}}_{\phi_E}\mathbb{Q}_{\varphi_p}\mathbb{D}_{\rho_p}\mathbb{Q}^{\mathrm{T}}_{\varphi_p}\mathbb{Q}_{\phi_E}\mathbb{S}_E\hat{x}\right)^{\frac{q(p+1)}{2}} h_E h_E^{\perp}\,\mathrm{d}\hat{x}.\end{aligned} \tag{3.42}$$

Let us put $\mathbb{G} := \mathbb{S}_E^{\mathrm{T}}\mathbb{Q}^{\mathrm{T}}_{\phi_E}\mathbb{Q}_{\varphi_p}\mathbb{D}_{\rho_p}\mathbb{Q}^{\mathrm{T}}_{\varphi_p}\mathbb{Q}_{\phi_E}\mathbb{S}_E$. Obviously, $\mathbb{G} \in \mathrm{Sym}$; cf. (2.4). Using the identity $\mathbb{Q}^{\mathrm{T}}_{\varphi_p}\mathbb{Q}_{\phi_E} = \mathbb{Q}_{\phi_E-\varphi_p} =: \mathbb{Q}_\tau$ (i.e., $\tau := \phi_E - \varphi_p$), we have $\mathbb{G} = \mathbb{S}_E^{\mathrm{T}}\mathbb{Q}_\tau^{\mathrm{T}}\mathbb{D}_{\rho_p}\mathbb{Q}_\tau\mathbb{S}_E$. The direct computation gives

$$\mathbb{Q}_\tau^{\mathrm{T}}\mathbb{D}_{\rho_p}\mathbb{Q}_\tau = \begin{pmatrix} \cos^2\tau + \rho_p^{-\frac{2}{p+1}}\sin^2\tau & -\sin\tau\cos\tau(1-\rho_p^{-\frac{2}{p+1}}) \\ -\sin\tau\cos\tau(1-\rho_p^{-\frac{2}{p+1}}) & \sin^2\tau + \rho_p^{-\frac{2}{p+1}}\cos^2\tau \end{pmatrix}, \tag{3.43}$$

and thus

$$\mathbb{G} = \begin{pmatrix} h_E^2(\cos^2\tau + \rho_p^{-\frac{2}{p+1}}\sin^2\tau) & -h_E h_E^{\perp}\sin\tau\cos\tau(1-\rho_p^{-\frac{2}{p+1}}) \\ -h_E h_E^{\perp}\sin\tau\cos\tau(1-\rho_p^{-\frac{2}{p+1}}) & (h_E^{\perp})^2(\sin^2\tau + \rho_p^{-\frac{2}{p+1}}\cos^2\tau) \end{pmatrix} \tag{3.44}$$

Using relation $\sigma_E = h_E/h_E^{\perp}$, we rewrite $\mathbb{G}$ by

$$\mathbb{G} = h_E h_E^{\perp}\bar{\mathbb{G}}, \quad \bar{\mathbb{G}} := \begin{pmatrix} \sigma_E(\cos^2\tau + \rho_p^{-\frac{2}{p+1}}\sin^2\tau) & -\sin\tau\cos\tau(1-\rho_p^{-\frac{2}{p+1}}) \\ -\sin\tau\cos\tau(1-\rho_p^{-\frac{2}{p+1}}) & \sigma_E^{-1}(\sin^2\tau + \rho_p^{-\frac{2}{p+1}}\cos^2\tau) \end{pmatrix}. \tag{3.45}$$

Therefore, (3.42), (3.45) and (3.41) give

$$\begin{aligned}\left\|e^{\mathrm{int}}_{\bar{x},p}\right\|^q_{L^q(E)} &\le A_p^q \left(h_E h_E^{\perp}\right)^{\frac{q(p+1)}{2}+1} \int_{\hat{E}} \left(\hat{x}^{\mathrm{T}}\bar{\mathbb{G}}\hat{x}\right)^{\frac{q(p+1)}{2}} \,\mathrm{d}\hat{x} \\ &= A_p^q \left(\frac{\nu_{\bar{x},p}}{\pi}\right)^{\frac{q(p+1)}{2}+1} \int_{\hat{E}} \left(\hat{x}^{\mathrm{T}}\bar{\mathbb{G}}\hat{x}\right)^{\frac{q(p+1)}{2}} \,\mathrm{d}\hat{x}.\end{aligned} \tag{3.46}$$

The inequality (3.46) gives the upper bound of the interpolation error function on the (up to now unknown) ellipse E in the L^q-norm depending on its area $\nu_{\bar{x},p}$, its aspect ratio σ_E and its orientation ϕ_E. These quantities can be used for an alternative definition of the anisotropy of E instead of (h_E, σ_E, ϕ_E). From the constrain (p2**), the value $\nu_{\bar{x},p}$ is given, hence we seek $\sigma_E \ge 1$ and $\phi_E \in [0, 2\pi)$, which minimize the estimate (3.46).

Let us deal with the integral on the right-hand side of (3.46). Let $\bar{g}_{i,j},\ i,j = 1,2$ denote the entries of $\bar{\mathbb{G}}$, i.e., $\bar{\mathbb{G}} = \{\bar{g}_{ij}\}_{i,j=1}^2$. We express the determinant of $\bar{\mathbb{G}}$ by

$$\begin{aligned}\det\bar{\mathbb{G}} =& (\cos^2\tau + \rho_p^{-\frac{2}{p+1}}\sin^2\tau)(\sin^2\tau + \rho_p^{-\frac{2}{p+1}}\cos^2\tau) \\ &- \left(\sin\tau\cos\tau(1-\rho_p^{-\frac{2}{p+1}})\right)^2 = \rho_p^{-\frac{2}{p+1}}.\end{aligned} \tag{3.47}$$

Moreover, since $\bar{\mathbb{G}} \in \mathrm{Sym}$, we can diagonalize it in the form $\bar{\mathbb{G}} = \mathbb{Q}_\psi^{\mathrm{T}} \mathbb{L} \mathbb{Q}_\psi$, where $\mathbb{Q}_\psi$ is the rotation through an angle ψ and $\mathbb{L} = \mathrm{diag}(L_1, L_2)$ where $L_i > 0,\ i = 1, 2$ are the eigenvalues of $\bar{\mathbb{G}}$. Furthermore, since $\mathbb{Q}_\psi$ is the rotation, it maps the reference circle $\hat{E}$ onto itself. (Here is the point, where it is advantageous to seek the ellipse E instead of the triangle K.) Hence, using the transformation $\hat{y} = \mathbb{Q}_\psi \hat{x}$, we have

$$\int_{\hat{E}} \left(\hat{x}^{\mathrm{T}} \bar{\mathbb{G}} \hat{x}\right)^{\frac{q(p+1)}{2}} \,\mathrm{d}\hat{x} = \int_{\hat{E}} \left(\hat{x}^{\mathrm{T}} \mathbb{Q}_\psi^{\mathrm{T}} \mathbb{L} \mathbb{Q}_\psi \hat{x}\right)^{\frac{q(p+1)}{2}} \,\mathrm{d}\hat{x} = \int_{\hat{E}} \left(\hat{y}^{\mathrm{T}} \mathbb{L} \hat{y}\right)^{\frac{q(p+1)}{2}} \,\mathrm{d}\hat{y}. \tag{3.48}$$

The eigenvalues $L_i,\ i = 1, 2$ of matrix of $\bar{\mathbb{G}}$ are the roots of the polynom

$$(\bar{g}_{11} - L)(\bar{g}_{22} - L) - \bar{g}_{12}^2 = L^2 - (\bar{g}_{11} + \bar{g}_{22})L + \bar{g}_{11}\bar{g}_{22} - \bar{g}_{12}^2 = 0,$$

hence

$$\begin{aligned} L_{1,2} &= \frac{\bar{g}_{11} + \bar{g}_{22}}{2} \pm \frac{1}{2}\sqrt{(\bar{g}_{11} + \bar{g}_{22})^2 - 4(\bar{g}_{11}\bar{g}_{22} - \bar{g}_{12}^2)} \\ &= \frac{\bar{g}_{11} + \bar{g}_{22}}{2} \pm \frac{1}{2}\sqrt{(\bar{g}_{11} - \bar{g}_{22})^2 + 4\bar{g}_{12}^2}. \end{aligned} \tag{3.49}$$

Moreover, since $\det \bar{\mathbb{G}} = \det \mathbb{L}$, we have due to (3.47) the equality $L_1 L_2 = \rho_p^{-\frac{2}{p+1}}$. Hence, we put

$$L_1 = a\delta, \quad L_2 = \frac{a}{\delta}, \tag{3.50}$$

where $a := \rho_p^{-\frac{1}{p+1}}$ is given and $\delta \geq 1$ is unknown.

In order to evaluate the last integral in (3.48), we use the polar coordinates, i.e., $\hat{y}_1 = r\cos t$, $\hat{y}_2 = r \sin t$. Then together with (3.50), we have

$$\begin{aligned} &\int_{\hat{E}} \left(\hat{y}^{\mathrm{T}} \mathbb{L} \hat{y}\right)^{\frac{q(p+1)}{2}} \,\mathrm{d}\hat{y} = \int_{\hat{E}} \left(L_1 \hat{y}_1^2 + L_2 \hat{y}_2^2\right)^{\frac{q(p+1)}{2}} \,\mathrm{d}\hat{y} \qquad (3.51) \\ &= \int_{r=0}^{1} \int_{t=0}^{2\pi} r^{q(p+1)} \left(L_1 \cos^2 t + L_2 \sin^2 t\right)^{\frac{q(p+1)}{2}} \, r \,\mathrm{d}t \,\mathrm{d}r \\ &= \int_{r=0}^{1} \int_{t=0}^{2\pi} r^{q(p+1)+1} a^{\frac{q(p+1)}{2}} \left(\delta \cos^2 t + \frac{1}{\delta} \sin^2 t\right)^{\frac{q(p+1)}{2}} \,\mathrm{d}t \,\mathrm{d}r =: D(\delta). \end{aligned}$$

We have to seek the value $\delta \geq 1$ such that $D(\delta)$ is minimal. We introduce the following auxiliary lemma which is proved in Appendix.

Lemma 3.13. *Let $s \geq 1$. We set*

$$S(\delta) := \int_{t=0}^{2\pi} \left(\delta \cos^2 t + \frac{1}{\delta} \sin^2 t\right)^s \,\mathrm{d}t, \qquad \delta \geq 1. \tag{3.52}$$

Then

$$S(\delta) > S(1) = 2\pi \quad \forall \delta > 1. \tag{3.53}$$

Lemma 3.13 implies that $D(\delta)$ defined by (3.51) is minimal for $\delta = 1$. Therefore, (3.50) gives $L_1 = L_2$ and consequently (3.49) implies that $\bar{g}_{11} = \bar{g}_{22}$ and $\bar{g}_{12} = 0$. From (3.45) we found that $\bar{g}_{12} = 0$ if either $\sin\tau = 0$ or $\cos\tau = 0$. Let us consider the latter case. Then

$$\begin{aligned} &\cos\tau = 0 \Rightarrow \tau = \phi_E - \varphi_p = \pi/2 \qquad (3.54) \\ &\qquad \text{and then} \quad \bar{g}_{11} = \bar{g}_{22} \Rightarrow \sigma_E \rho_p^{-\frac{2}{p+1}} = \sigma_E^{-1} \ \Rightarrow \sigma_E = \rho_p^{\frac{1}{p+1}}. \end{aligned}$$

For the former case $\sin\tau = 0$ we have

$$\sin\tau = 0 \Rightarrow \tau = \phi_E - \varphi_p = 0 \tag{3.55}$$
$$\text{and then} \quad \bar{g}_{11} = \bar{g}_{22} \Rightarrow \sigma_E = \sigma_E^{-1}\rho_p^{-\frac{2}{p+1}} \Rightarrow \sigma_E = \rho_p^{-\frac{1}{p+1}},$$

which is a unacceptable case because $\rho_p^{-\frac{1}{p+1}} \leq 1$ and we require $\sigma_E \geq 1$. Therefore, (3.54) defines the aspect ratio σ_E and orientation ϕ_E of element E satisfying condition (p1**) and (p2**) presented at the beginning of this section. The area of this element satisfies (3.41), hence $h_E = (\sigma_E \nu_{\bar{x},p}/\pi)^{1/2}$. We observe that the orientation ϕ_E of the sought ellipse E is perpendicular to the orientation of the interpolation error function φ_p, i.e., the "element is small" along the direction of the highest directional derivative $\mathrm{d}^{p+1}u(\bar{x};\cdot)$, which is in agreement with the general expectation.

Furthermore, from (3.54), we have $\bar{g}_{11} = \bar{g}_{22} = \rho_p^{-\frac{1}{p+1}}$ and thus

$$\bar{\mathbb{G}} := \begin{pmatrix} \rho_p^{-\frac{1}{p+1}} & 0 \\ 0 & \rho_p^{-\frac{1}{p+1}} \end{pmatrix}. \tag{3.56}$$

Moreover, (3.48) and (3.51) (together with $\delta = 1$) gives

$$\int_{\hat{E}} \left(\hat{x}^{\mathrm{T}}\bar{\mathbb{G}}\hat{x}\right)^{\frac{q(p+1)}{2}} \mathrm{d}\hat{x} = 2\pi \int_0^1 r^{q(p+1)+1} (\rho_p^{-\frac{1}{p+1}})^{\frac{q(p+1)}{2}} \mathrm{d}r = \frac{2\pi\, \rho_p^{-\frac{q}{2}}}{q(p+1)+2}. \tag{3.57}$$

Finally, from (3.46) and (3.57), we have

$$\left\|e^{\mathrm{int}}_{\bar{x},p}\right\|^q_{L^q(E)} \leq A_p^{\,q} \left(\frac{\nu_{\bar{x},p}}{\pi}\right)^{\frac{q(p+1)}{2}+1} \frac{2\pi\, \rho_p^{-\frac{q}{2}}}{q(p+1)+2}. \tag{3.58}$$

Then

$$\left\|e^{\mathrm{int}}_{\bar{x},p}\right\|_{L^q(E)} \leq c_{p,q} A_p \rho_p^{-\frac{1}{2}} \left((\nu_{\bar{x},p})^{\frac{q(p+1)}{2}+1}\right)^{1/q} \tag{3.59}$$

with $c_{p,q} := \left(\frac{2\pi}{q(p+1)+2}\left(\frac{1}{\pi}\right)^{\frac{q(p+1)}{2}+1}\right)^{1/q}$ gives the estimate of the interpolation error function $e^{\mathrm{int}}_{\bar{x},p}$ in the L^q-norm on the optimal ellipse E with the anisotropy

$$h_E = \left(\rho_p^{\frac{1}{p+1}} \frac{\nu_{\bar{x},p}}{\pi}\right)^{1/2}, \quad \sigma_E = \rho_p^{\frac{1}{p+1}}, \quad \phi_E = \varphi_p - \pi/2, \tag{3.60}$$

as follows from (3.41) and (3.54). Therefore, we conclude that the ellipse E with the barycentre $\bar{x}$ and the anisotropy $\{h_E, \sigma_E, \phi_E\}$ given by (3.60) satisfies the conditions (p1**) and (p2**) presented at the beginning of this section.

Moreover, we expect that if K is the triangle with the same barycentre $\bar{x}$ and having the same anisotropy $\{h_E, \sigma_E, \phi_E\}$ as the ellipse E, then K is the solution of Problem 3.4. In Section 2.2, we mentioned the equivalency between a triangle and the corresponding ellipse, they areas are equal up to a multiplicative constant.

3.3.2 Estimate in the L^∞-norm

The estimate the L^∞-norm is more simple, we follow the approach from the previous section. Instead of (3.42), we have

$$\left\|e^{\mathrm{int}}_{\bar{x},p}\right\|_{L^\infty(E)} = \max_{x\in E} \left|e^{\mathrm{int}}_{\bar{x},p}(x)\right| \leq \max_{x\in E} A_p \left((x-\bar{x})^{\mathrm{T}} \mathbb{Q}_{\varphi_p} \mathbb{D}_{\rho_p} \mathbb{Q}^{\mathrm{T}}_{\varphi_p} (x-\bar{x})\right)^{\frac{p+1}{2}} \tag{3.61}$$
$$= \max_{\hat{x}\in\hat{E}} A_p \left(\hat{x}^{\mathrm{T}} \mathbb{S}_E^{\mathrm{T}} \mathbb{Q}^{\mathrm{T}}_{\phi_E} \mathbb{Q}_{\varphi_p} \mathbb{D}_{\rho_p} \mathbb{Q}^{\mathrm{T}}_{\varphi_p} \mathbb{Q}_{\phi_E} \mathbb{S}_E \hat{x}\right)^{\frac{p+1}{2}}.$$

Using (3.43) – (3.48), we obtain

$$\left\|e^{\mathrm{int}}_{\bar{x},p}\right\|_{L^\infty(E)} \le A_p \left(h_E h_E^{\perp}\right)^{\frac{p+1}{2}} \max_{\hat{x}\in\hat{E}} \left(\hat{x}^{\mathrm{T}}\bar{\mathbb{G}}\hat{x}\right)^{\frac{p+1}{2}} = A_p \left(\frac{\nu_{\bar{x},p}}{\pi}\right)^{\frac{p+1}{2}} \max_{\hat{y}\in\hat{E}} \left(\hat{y}^{\mathrm{T}}\mathbb{L}\hat{y}\right)^{\frac{p+1}{2}}, \tag{3.62}$$

where $\mathbb{L}$ is the diagonal matrix with eigenvalues satisfying (3.50). Obviously, the term

$$\max_{\hat{y}\in\hat{E}} \left(\hat{y}^{\mathrm{T}}\mathbb{L}\hat{y}\right)^{\frac{p+1}{2}} = \max_{\hat{y}\in\hat{E}} \left(L_1\hat{y}_1^2 + L_2\hat{y}_2^2\right)^{\frac{p+1}{2}}$$

is minimal for $L_1 = L_2$. Hence using (3.54) – (3.55) we obtain that the element with the anisotropy given by (3.60) satisfies conditions (p1**) and (p2**). Finally, (3.54) gives (3.56) also for $q = \infty$ and then

$$\hat{x}^{\mathrm{T}}\bar{\mathbb{G}}\hat{x} = \rho_p^{-\frac{1}{p+1}} \quad \forall|\hat{x}| = 1,$$

which together with (3.61) gives

$$\left\|e^{\mathrm{int}}_{\bar{x},p}\right\|_{L^\infty(E)} \le A_p \left(\frac{\nu_{\bar{x},p}}{\pi}\right)^{\frac{p+1}{2}} \max_{\hat{x}\in\hat{E}} \left(\hat{x}^{\mathrm{T}}\bar{\mathbb{G}}\hat{x}\right)^{\frac{p+1}{2}} = A_p\rho_p^{-\frac{1}{2}} \left(\frac{\nu_{\bar{x},p}}{\pi}\right)^{\frac{p+1}{2}}. \tag{3.63}$$

Similarly as in Section 3.3.1, the triangle K having the anisotropy (3.60) is the solution of the auxiliary Problem 3.4 for $q = \infty$ and the minimal error is given by (3.63).

3.3.3 Solution of the auxiliary Problem 3.4

Finally, due to the equivalency of Problems 3.3 and 3.4, using (3.59), (3.60) and (3.63), we obtain the solution of Problem 3.3 which is formulated in the following Lemma.

Lemma 3.14. *Let $u \in V$, $\bar{x} \in \Omega$, $p \in \mathbb{N}$, $q \in [1,\infty]$ and $\bar{\omega} > 0$ be given. Let $\{A_p, \varphi_p, \rho_p\}$ defined by* (3.33) *be the anisotropy of the corresponding interpolation error function $e^{\mathrm{int}}_{\bar{x},p}$. We set $\nu_{\bar{x},p}$ by*

$$\begin{aligned}
&\nu_{\bar{x},p} := \left(\frac{\bar{\omega}\rho_p^{\frac{1}{2}}}{c_{p,q}A_p}\right)^{\frac{2q}{q(p+1)+2}} \quad \Longrightarrow \quad \bar{\omega} = c_{p,q}A_p\rho_p^{-\frac{1}{2}} \left(\nu_{\bar{x},p}\right)^{\frac{q(p+1)+2}{2q}}, \quad \text{for } q \in [1,\infty),\\
&\nu_{\bar{x},p} := \left(\frac{\bar{\omega}\rho_p^{\frac{1}{2}}}{A_p}\right)^{\frac{2}{p+1}} \quad \Longrightarrow \quad \bar{\omega} = A_p\rho_p^{-\frac{1}{2}} \left(\nu_{\bar{x},p}\right)^{\frac{p+1}{2}}, \quad \text{for } q = \infty,
\end{aligned} \tag{3.64}$$

where $c_{p,q}$ appears in (3.59). *Then the triangle $K_{\bar{x},p}$ with the anisotropy $\{h_E, \sigma_E, \phi_E\}$ given by*

$$h_E = \left(\rho_p^{\frac{1}{p+1}}\,\frac{\nu_{\bar{x},p}}{\pi}\right)^{1/2}, \quad \sigma_E = \rho_p^{\frac{1}{p+1}}, \quad \phi_E = \varphi_p - \pi/2 \tag{3.65}$$

is the solution of Problem 3.3. *Moreover, we have the bound*

$$\left\|e^{\mathrm{int}}_{\bar{x},p}\right\|_{L^q(K_{\bar{x},p})} \le \bar{\omega}. \tag{3.66}$$

Let us note that $\bar{\omega}$ can be considered as a *local* tolerance for each element K and it will be specified in Section 4.

4 Solution of the main Problem 3.2

We proceed to the solution of the main Problem 3.2. We have already mentioned, we are not able to solve Problem 3.2 exactly. However, with the aid of the auxiliary Problem 3.3, we derive a Riemann metric $\mathcal{M} : \Omega \to \mathrm{Sym}$ and a polynomial degree distribution function $\mathcal{P} : \Omega \to \mathbb{R}^+$, which define the *hp*-mesh $\mathscr{T}_{hp}$ (by Definitions 2.8 and 2.9). This *hp*-mesh satisfies condition (P1) of Problem 3.2 and the corresponding number of degrees of freedom is small. Therefore, we expect that this resulting *hp*-mesh is close to the (hypothetical) solution of Problem 3.2.

We define formally the optimal mesh as a mesh, whose each element K is the solution of the auxiliary Problem 3.3 considered at the barycentre of K. Lemma 3.14 gives the anisotropy (the size, the aspect ration and the orientation) of the "optimal triangle" with the barycentre at any $\bar{x} \in \Omega$, the anisotropy depends on the local tolerance $\bar{\omega}$. Therefore, we need to specify the size of $\bar{\omega}$ (or the area $\nu_{\bar{x},p}$) in (3.64) in such a way that the interpolation error over Ω is under the given (global) tolerance ω.

Moreover, we need to specify the polynomial approximation degree for each element of the mesh, i.e., we have to define the polynomial degree distribution function $\mathcal{P}$. Hence, with respect to Remark 2.10, we find the optimal degree of the polynomial approximation for each $\bar{x} \in \Omega$.

4.1 Setting of the local tolerance

The main Problem 3.2 requires the error bound

$$\|u - \Pi_{h\mathsf{p}} u\|_{L^q(\Omega)} \leq \omega, \tag{4.1}$$

where $\omega > 0$ is the given (global) tolerance.

First, we consider the case $q \in [1, \infty)$. Obviously, the condition (4.1) will be satisfied if

$$\|u - \Pi_{h\mathsf{p}} u\|_{L^q(K)} \leq \omega \left(\frac{|K|}{|\Omega|}\right)^{\frac{1}{q}} \qquad \forall K \in \mathscr{T}_h, \tag{4.2}$$

because then $\|u - \Pi_{h\mathsf{p}} u\|^q_{L^q(\Omega)} = \sum_{K \in \mathscr{T}_h} \|u - \Pi_{h\mathsf{p}} u\|^q_{L^q(K)} \leq \omega^q \sum_{K \in \mathscr{T}_h} \frac{|K|}{|\Omega|} = \omega^q$.

We employ (4.2) for the setting of the local tolerance $\bar{\omega}$ in (3.64). Let $\bar{x} \in \Omega$ and $p \geq 1$ be given and let $K_{\bar{x},p}$ denote the triangle which is the solution of Problem 3.3 given by Lemma 3.14 with the (so far unknown) local tolerance $\bar{\omega}$. Then, from (3.64) and (3.66), we have the estimate

$$\left\|e^{\mathrm{int}}_{\bar{x},p}\right\|_{L^q(K_{\bar{x},p})} \leq c_{p,q} A_p \rho_p^{-\frac{1}{2}} \left(\nu_{\bar{x},p}\right)^{\frac{q(p+1)+2}{2q}}, \tag{4.3}$$

where $\nu_{\bar{x},p}$ denotes the area of $K_{\bar{x},p}$ which we are going to specify. In virtue of (3.6) and (4.2), we require that

$$\left\|e^{\mathrm{int}}_{\bar{x},p}\right\|_{L^q(K_{\bar{x},p})} \leq \omega \left(\frac{\nu_{\bar{x},p}}{|\Omega|}\right)^{\frac{1}{q}}. \tag{4.4}$$

Hence, in order to specify area $\nu_{\bar{x},p}$, using (4.3) – (4.4), we set the condition

$$c_{p,q} A_p \rho_p^{-\frac{1}{2}} \left(\nu_{\bar{x},p}\right)^{\frac{q(p+1)+2}{2q}} = \omega \left(\frac{\nu_{\bar{x},p}}{|\Omega|}\right)^{\frac{1}{q}}. \tag{4.5}$$

From the equality (4.5), we obtain

$$\left(\nu_{\bar{x},p}\right)^{\frac{q(p+1)}{2q}} = \frac{\omega \rho_p^{\frac{1}{2}}}{c_{p,q} A_p |\Omega|^{\frac{1}{q}}} \quad \Longleftrightarrow \quad \nu_{\bar{x},p} = |\Omega|^{-\frac{2}{q(p+1)}} \left(\frac{\omega \rho_p^{\frac{1}{2}}}{c_{p,q} A_p}\right)^{\frac{2}{p+1}}. \tag{4.6}$$

Finally, inserting (4.6) into the second relation of (3.64), we have

$$\bar{\omega} = c_{p,q} A_p \rho_p^{-\frac{1}{2}} |\Omega|^{-\frac{q(p+1)+2}{q^2(p+1)}} \left(\frac{\omega \rho_p^{\frac{1}{2}}}{c_{p,q} A_p}\right)^{\frac{q(p+1)+2}{q(p+1)}}, \ q \in [1, \infty). \tag{4.7}$$

For the case $q = \infty$, we have $\|u - \Pi_{h\mathsf{p}} u\|_{L^\infty(\Omega)} = \max_{K \in \mathscr{T}_h} \|u - \Pi_{h\mathsf{p}} u\|_{L^\infty(K)}$. Hence, instead of (4.2), we require

$$\|u - \Pi_{h\mathsf{p}} u\|_{L^\infty(K)} \leq \omega \quad \forall K \in \mathscr{T}_h. \tag{4.8}$$

Therefore, we put $\bar{\omega} := \omega$ and from (3.64), we get

$$\nu_{\bar{x},p} = \left(\frac{\omega \rho_p^{\frac{1}{2}}}{A_p} \right)^{\frac{2}{p+1}}, \quad q = \infty. \tag{4.9}$$

We summarize the previous derivation in the following lemma.

Lemma 4.1. *Let $u \in V$, $\bar{x} \in \Omega$, $p \in \mathbb{N}$, $q \in [1, \infty]$ and $\omega > 0$ be given. Let $\{A_p, \varphi_p, \rho_p\}$, defined by (3.33), be the anisotropy of the corresponding interpolation error function $e^{\mathrm{int}}_{\bar{x},p}$. Let $K_{\bar{x},p}$ be the triangle with the anisotropy $\{h_E, \sigma_E, \phi_E\}$ defined by (3.65), where its area $\nu_{\bar{x},p}$ is given by (4.6) for $q \in [1, \infty)$ and by (4.9) for $q = \infty$. Then, we have the bounds*

$$\left\| e^{\mathrm{int}}_{\bar{x},p} \right\|_{L^q(K_{\bar{x},p})} \leq \omega \left(\frac{\nu_{\bar{x},p}}{|\Omega|} \right)^{\frac{1}{q}} \quad q \in [1, \infty) \qquad \text{or} \qquad \left\| e^{\mathrm{int}}_{\bar{x},p} \right\|_{L^\infty(K_{\bar{x},p})} \leq \omega. \tag{4.10}$$

The meaning of Lemma 4.1 is the following. Let $\mathscr{T}_h$ be a hypothetical triangulation of Ω whose all triangles K are the solutions of Problem 3.3 considered at $\bar{x} := x_K \; \forall K \in \mathscr{T}_h$, ($x_K$ is the barycentre of K) for given $u \in V$ and $p \geq 1$ with $\bar{\omega}$ given by (4.7) for $q \in [1, \infty)$ and $\bar{\omega} := \omega$ for $q = \infty$. Then

$$\sum_{K \in \mathscr{T}_h} \left\| e^{\mathrm{int}}_{\bar{x},p} \right\|^q_{L^q(K)} \leq \omega^q \sum_{K \in \mathscr{T}_h} \frac{\nu_{\bar{x},p}}{|\Omega|} = \omega^q, \; q \in [1, \infty) \quad \text{or} \quad \max_{K \in \mathscr{T}_h} \left\| e^{\mathrm{int}}_{\bar{x},p} \right\|_{L^\infty(K)} \leq \omega, \tag{4.11}$$

and all $K \in \mathscr{T}_h$ has the optimal size, orientation and aspect ratio in the sense of Problem 3.3.

4.2 Choice of the degree of the polynomial approximation

In Sections 3.3 and 4.1, we have derived the anisotropy of the optimal triangle $K_{\bar{x},p}$, which minimizes the norm of the interpolation error function $e^{\mathrm{int}}_{\bar{x},p}$ on $K_{\bar{x},p}$ for any $\bar{x} \in \Omega$ and for the arbitrary given polynomial approximation degree p. In this section, we discuss the question which degree p is the optimal one.

Let $\bar{x} \in \Omega$ and $K_{\bar{x},p}$, $p \in \mathbb{N}$ be the solutions of Problem 3.3 given by Lemma 3.14 for all $p \in \mathbb{N}$. In virtue of (3.39), (3.65) and Definition 2.2, this triangle is generated by the matrix

$$\mathbb{M}_{\bar{x},p} = \frac{\pi}{\nu_{\bar{x},p}} \rho_p^{-\frac{1}{p+1}} \, \mathbb{Q}^{\mathrm{T}}_{\phi_E} \begin{pmatrix} 1 & 0 \\ 0 & \rho_p^{\frac{2}{p+1}} \end{pmatrix} \mathbb{Q}_{\phi_E}. \tag{4.12}$$

Obviously, $(\det \mathbb{M}_{\bar{x},p})^{-1/2} = \frac{\nu_{\bar{x},p}}{\pi}$, which is in agreement with (2.9) up to the multiplicative constant. The difference follows from the fact that the estimate derived for the ellipse E in Section 3.3 was used for the corresponding triangle.

In Section 2.4, we introduced the so-called *"density of the number of degrees of freedom"* $\eta(x)$ by the ratio of the number of degrees of freedom $d(x)$ and the volume ($\approx (\det \mathcal{M}(x))^{1/2}$), $x \in \Omega$. Hence, we define its analogue

$$\eta_p(\bar{x}) := \frac{2}{3\sqrt{3}} (p+1)(p+2) \, (\det \mathbb{M}_{\bar{x},p})^{1/2} = \frac{2\pi}{3\sqrt{3}} \frac{(p+1)(p+2)}{\nu_{\bar{x},p}}, \quad p \in \mathbb{N}, \; \bar{x} \in \Omega. \tag{4.13}$$

Then, the analogue to the generalized number of degrees of freedom (2.23) is

$$\int_\Omega \eta_p(\bar{x}) \mathrm{d}\bar{x}. \tag{4.14}$$

Therefore, in order to minimize (4.14), we choose, for each $\bar{x} \in \Omega$, the polynomial degree $p \in \mathbb{N}$ such that the corresponding value $\eta_{\bar{x},p}$ is minimal, i.e., we set

$$p_{\bar{x}} := \arg \min_{p \in \mathbb{N}} \eta_p(\bar{x}). \tag{4.15}$$

Let us note that in practical implementation, the degree p is bounded from above by the maximal implemented polynomial approximation degree, hence the minimum in (4.15) always exists.

4.3 Setting of the optimal anisotropic hp-mesh

Now we are ready to define the Riemann metric $\mathcal{M}$ and the polynomial degree distribution function $\mathcal{P}$, which generate the hp-mesh $\mathscr{T}_{h\mathsf{p}}$ by Definitions 2.8 and 2.9, such that $\mathscr{T}_{h\mathsf{p}}$ is close to the solution of the main Problem 3.2. Using the derivations from the previous section, we derive the following algorithm.

Algorithm (A) (Generation of $\mathcal{M}(x)$ and $\mathcal{P}(x)$ for $x \in \Omega$)
Let $u \in V$, $q \in [1, \infty]$ and $\omega > 0$ be given. Then

1. For each $p = 1, 2, \dots,$

   (a) We evaluate the anisotropy of the interpolation error function at x with the aid of (3.33) with $\bar{x} := x$, we set the quantities $A_p(x) := A_p$, $\varphi_p(x) := \varphi_p$ and $\rho_p(x) = \rho_p$.

   (b) Using (4.6) and (4.9), we set the area $\nu_p(x)$ of the triangle $K_{x,p}$ by

   $$\nu_p(x) := |\Omega|^{-\frac{2}{q(p+1)}} \left(\omega \rho_p^{\frac{1}{2}}(x) c_{p,q}^{-1} {A_p}^{-1}(x)\right)^{\frac{2}{p+1}} \qquad \text{for } q \in [1, \infty),$$
   $$\nu_p(x) := \left(\frac{\omega \rho_p^{\frac{1}{2}}}{A_p}\right)^{\frac{2}{p+1}} \qquad \text{for } q = \infty,$$

   with $c_{p,q}$ from (3.59).

   (c) Analogously to relation (3.65), we define the optimal anisotropy of $K_{x,p}$ by the triple $\{h_E(x), \sigma_E(x), \phi_E(x)\}$ given by

   $$h_E(x) := \left(\rho_p^{\frac{1}{p+1}}(x) \frac{\nu_p(x)}{\pi}\right)^{1/2}, \ \sigma_E(x) := \rho_p^{\frac{1}{p+1}}(x), \ \phi_E(x) := \varphi_p(x) - \pi/2,$$

   (d) Using (3.39) we set

   $$\mathbb{M}_p(x) := \frac{1}{h_E(x)^2} \mathbb{Q}^{\mathrm{T}}_{\phi_E(x)} \begin{pmatrix} 1 & 0 \\ 0 & \sigma_E(x)^2 \end{pmatrix} \mathbb{Q}_{\phi_E(x)}. \tag{4.16}$$

   (e) Using (4.13), we evaluate the quantity $\eta_p(x) := \frac{2\pi}{3\sqrt{3}} \frac{(p+1)(p+2)}{\nu_p(x)}$.

2. We find $p_x \in \mathbb{N}$ minimizing $\eta_p(x)$, i.e. $p_x := \arg\min_{p \in \mathbb{N}} \eta_p(x)$.

3. We set

   $$\mathcal{M}(x) := \mathbb{M}_{p_x}(x), \quad \mathcal{P}(x) := p_x.$$

   where $\mathbb{M}_{p_x}(x)$ is given by (4.16).

Theoretically, we can employ the previous algorithm for any $x \in \Omega$. In practical application, we evaluate $\mathcal{M}$ and $\mathcal{P}$ only for the finite number of $x \in \Omega$ and then we continuously interpolate $\mathcal{M}$ and $\mathcal{P}$ on Ω.

5 Numerical implementation

In previous sections, we developed the algorithm, which generates, for a given function u, the anisotropic hp-grid such that the interpolation error is under the given tolerance and the number of degrees of freedom $N_{h\mathsf{p}}$ is small. We apply this algorithm for the numerical solution of a boundary value problem (BVP).

Let $u : \Omega \to \mathbb{R}$ be the exact solution of the given BVP. The goal is to find a hp-mesh (and the corresponding space $S_{h\mathsf{p}}$ given by (2.2)) such that the approximate solution $u_{h\mathsf{p}} \in S_{h\mathsf{p}}$ satisfies $\|u - u_{h\mathsf{p}}\|_{L^q(\Omega)} \le \omega$ and the corresponding $N_{h\mathsf{p}}$ is small. The final (optimal) hp-grid is obtained iteratively after several adaptations with the aid of Algorithm (A) from Section 4.3. Particularly,

if $u_{h\mathsf{p}}$ is an approximate solution of BVP obtained on the given hp-mesh $\mathscr{T}_{h\mathsf{p}}$ then we generate a new (better) mesh $\mathscr{T}_{h\mathsf{p}}^N$ where the more accurate approximate solution can be obtained. In the following we describe the implementation of Algorithm (A) with the aid of the software package ANGENER [14]. If a triangular grid $\mathscr{T}_h$ is given together with the metric $\mathcal{M}$ evaluated at the barycentres x_K of all $K \in \mathscr{T}_h$, then ANGENER creates a new anisotropic triangular grid in the sense of Definition 2.8. Therefore, for our purposes, it is sufficient to perform Algorithm (A) only for $x_K,\ K \in \mathscr{T}_h$.

Furthermore, since the optimal mesh is sought iteratively, it makes no sense to test all possible polynomial approximation degrees in the step (1) of Algorithm (A). We use the following strategy. If K is an element from the initial mesh $\mathscr{T}_{h\mathsf{p}}$ and p_K the corresponding polynomial approximation degree then we perform the step (1) of Algorithm (A) only for $p := p_K - 1$, $p := p_K$ and $p := p_K + 1$.

Moreover, in the step (a) of Algorithm (A), we approximate the $p+1$ directional derivative of u for $p = p_K - 1, p_K, p_K + 1$ in the following way. For each $K \in \mathscr{T}_h$, we define the patch $D(K)$ which consists of all $K' \in \mathscr{T}_h$ sharing a face with K. Then we define the polynomial function $\tilde{u}_{K,p} \in P^{p+1}(D(K))$ by

$$(\tilde{u}_{K,p}, \phi)_{1,D(K)} = (u_{h\mathsf{p}}, \phi)_{1,D(K)} \quad \forall \phi \in P^{p+1}(D(K)), \tag{5.1}$$

where $P^{p+1}(D(K))$ is the space of polynomial functions of degree $p+1$ on $D(K)$ and $(\cdot,\cdot)_{1,D(K)}$ is the H^1-scalar product on $D(K)$. Then the partial derivative of degree $p+1$ of $\tilde{u}_{K,p}$ are constant on K and in step (a) of Algorithm (A), where we evaluate A_p, φ_p and ρ_p by (3.33), we replace u by $\tilde{u}_{K,p}$.

Hence, the output of the implemented algorithm are

$$\mathcal{M}(x_K) \in \mathrm{Sym}, \quad \mathcal{P}(x_K) \in \mathbb{N}, \qquad \forall K \in \mathscr{T}_h. \tag{5.2}$$

The matrices $\mathcal{M}(x_K),\ K \in \mathscr{T}_h$ are passed to ANGENER which generates a new mesh $\mathscr{T}_h^N$. Finally, for each vertex x_P of the old mesh $\mathscr{T}_h$, we set $\mathcal{P}(x_P) \in \mathbb{R}^+$ as the average of $\mathcal{P}(x_K)$ for all K having x_P as a vertex. Then, we obtain a continuous piecewise linear function $\mathcal{P} : \Omega \to \mathbb{R}^+$ on $\mathscr{T}_h$ and using (2.15) we compute the polynomial approximation degrees on the new mesh $\mathscr{T}_h^N$.

6 Numerical experiments

In this Section, we present several numerical examples, which demonstrate the efficiency of the proposed anisotropic hp-adaptive method. The goal is to compare the proposed anisotropic hp-adaptive method with the isotropic hp-adaptive method presented in [17], where the exponential rate of the convergence was numerically justified. Moreover, we apply the presented technique to the solution of more complicated problems with multiple curved interior layers.

We apply Algorithm (A) from previous Section to the numerical solution of boundary value problems (BVPs), which are solved with the aid of the *discontinuous Galerkin method* (DGM). It approximates the solution by a function from the space of discontinuous piecewise polynomial functions $S_{h\mathsf{p}}$. We employ the incomplete interior penalty Galerkin (IIPG) variant of DGM, which was analysed in several papers [11, 40, 16]. We do not present here the discretization of BVP by IIPG, we refer to [17].

We consider the following examples:

(E1) linear convection-diffusion equation with boundary layers from [10], [20],

(E2) nonlinear convection-diffusion equation with a corner singularity from [30],

(E3) quasi-linear elliptic problem with a corner singularity from [28], [41],

(E4) convection-dominated problem with two curved interior layers from [32],

(E5) a generalization of (E4) with three curved interior layers.

For the cases (E1) – (E3), we know the exact analytical solution and therefore we are able to evaluate the computational error $e_{h\mathsf{p}} = u - u_{h\mathsf{p}}$, where u is the exact solution and $u_{h\mathsf{p}} \in S_{h\mathsf{p}}$ the approximate one. For examples (E1) – (E3), we carried out three types of the mesh adaptation:

- isotropic *hp*-adaptive algorithm from [17], which is based on the residual error estimates measured in the H^1-dual norm,
- anisotropic *hp*–adaptive algorithm (A) from Sections 4 – 5 for $q = \infty$,
- anisotropic *hp*–adaptive algorithm (A) from Sections 4 – 5 for $q = 2$.

For each case, we carried out several adaptation levels $\ell = 0, 1, \dots$ until the corresponding estimate is under the prescribed tolerance. For the isotropic adaptation we chose the tolerance similarly as in [17]. For the anisotropic adaptations, we set the tolerance ω such that the final numerical solution has the computational errors approximately equal to the errors obtained by the isotropic adaptation.

The results are given in Tables 1 – 4, where we present (for each level of adaptation $\ell = 0, 1, \dots$) the numbers of triangles N_h of the mesh $\mathscr{T}_h$, the numbers of degrees of freedom $N_{h\mathsf{p}}$ of the *hp*-mesh $\mathscr{T}_{h\mathsf{p}}$, the computational errors $e_{h\mathsf{p}}$ in the L^∞-norm, the L^2-norm and the H^1-norm. Moreover, we present the values of the corresponding error estimators ("estim"), i.e., the residual error estimator for the isotropic adaptive algorithm and the values $\left\|e^{\mathrm{int}}_{\bar{x},p}\right\|_{L^q(\Omega)}$, $q = \infty$ and $q = 2$ for the anisotropic adaptations, respectively. Furthermore, we evaluate the corresponding experimental orders of convergence (EOC) with respect to $N_{h\mathsf{p}}$ given by

$$\mathrm{EOC} = \frac{\log e^{(\ell+1)}_{h\mathsf{p}} - \log e^{(\ell)}_{h\mathsf{p}}}{\log\left(1/\sqrt{\log N^{(\ell+1)}_{h\mathsf{p}}}\right) - \log\left(1/\sqrt{N^{(\ell)}_{h\mathsf{p}}}\right)}, \qquad \ell = 1, 2, \dots, \tag{6.1}$$

where $e^{(\ell)}_{h\mathsf{p}}$, $\ell = 0, 1, \dots$ is either the computational error in the appropriate norm or the estimator after ℓ levels of mesh adaptation and $N^{(\ell)}_{h\mathsf{p}}$, $\ell = 0, 1, \dots$ is the corresponding number of degrees of freedom.

Sometimes, EOC are negative, namely in cases, when the error is decreasing even for the decreasing number of degrees of freedom. It is in fact an advantage of the presented technique that it can reduce the number of degrees of freedom as well as the computational error.

The main goal is to compare the number of degrees of freedom $N_{h\mathsf{p}}$ for the three presented adaptive techniques. Let us note that in same cases, the computational time is larger for the anisotropic adaptations than for the isotropic one even if $N_{h\mathsf{p}}$ is smaller. This follows from the fact that the construction of the anisotropic grids requires roughly the same computational time as the itself solution of BVP by DGM. However, for more complex problems, e.g., computational fluid dynamics, the construction of the anisotropic *hp*-grids becomes negligible in comparison to the DG solver.

For the examples (E4) – (E5), the analytical solution is unknown. However, we employ them to demonstrate the ability of the proposed algorithm to solve more complicated problems with thin curved interior layers. Let us note that we do not use any additional stabilization technique for capturing of boundary or interior layers. Finally, the solution of the examples (E4) – (E5) by the isotropic adaptation is almost impossible using a standard PC since the number of degrees of freedom is enormous, hence we do not present them.

6.1 (E1): Linear convection-diffusion equation with boundary layers

We consider the scalar linear convection-diffusion equation (similarly as in [10], [20])

$$-\varepsilon \triangle u - \frac{\partial u}{\partial x_1} - \frac{\partial u}{\partial x_2} = g \quad \text{in } \Omega := (0,1)^2, \tag{6.2}$$

isotropic *hp*-adaptation

ℓ	N_h	N_{hp}	$\|e_{hp}\|_{L^\infty}$	EOC	$\|e_{hp}\|_{L^2}$	EOC	$\|e_{hp}\|_{H^1}$	EOC	estim	EOC
0	128	384	5.03E-01	–	6.19E-02	–	3.88E+00	–	1.04E+01	–
1	128	768	3.40E-01	1.1	3.46E-02	1.7	3.90E+00	-0.0	6.09E+00	1.5
2	128	1232	2.49E-01	1.3	1.92E-02	2.5	2.51E+00	1.9	3.41E+00	2.5
3	158	1922	5.09E-02	7.1	7.03E-03	4.5	1.20E+00	3.3	1.63E+00	3.3
4	236	3392	2.20E-02	3.0	1.56E-03	5.3	3.72E-01	4.1	4.83E-01	4.3
5	380	6236	9.74E-03	2.7	1.88E-04	6.9	6.93E-02	5.5	7.41E-02	6.2
6	554	10308	1.09E-03	8.7	1.44E-05	10.2	7.85E-03	8.7	8.40E-03	8.7
7	770	16820	7.31E-05	11.0	7.57E-07	12.0	5.80E-04	10.6	5.73E-04	11.0
8	854	19812	3.25E-05	9.9	1.03E-06	-3.7	3.77E-04	5.3	3.91E-04	4.7

anisotropic *hp*-adaptation using the L^∞-norm

ℓ	N_h	N_{hp}	$\|e_{hp}\|_{L^\infty}$	EOC	$\|e_{hp}\|_{L^2}$	EOC	$\|e_{hp}\|_{H^1}$	EOC	estim	EOC
0	64	960	1.73E-01	–	1.34E-02	–	1.71E+00	–	1.27E+00	–
1	130	1950	4.63E-02	3.7	2.02E-03	5.3	3.89E-01	4.2	2.32E-01	4.8
2	156	2358	4.69E-03	24.1	1.69E-04	26.1	3.63E-02	25.0	3.35E-02	20.4
3	194	3060	2.55E-04	22.4	1.20E-05	20.3	2.19E-03	21.5	3.48E-03	17.4
4	271	4492	5.07E-05	8.4	3.37E-06	6.6	6.17E-04	6.6	3.43E-03	0.1
5	301	5343	3.58E-05	4.0	2.02E-06	5.9	3.02E-04	8.2	2.82E-04	28.8
6	308	5655	3.57E-05	0.0	1.94E-06	1.5	2.75E-04	3.4	1.34E-04	26.3

anisotropic *hp*-adaptation using the L^2-norm

ℓ	N_h	N_{hp}	$\|e_{hp}\|_{L^\infty}$	EOC	$\|e_{hp}\|_{L^2}$	EOC	$\|e_{hp}\|_{H^1}$	EOC	estim	EOC
0	64	960	1.73E-01	–	1.34E-02	–	1.71E+00	–	4.71E-02	–
1	160	2466	3.10E-02	3.6	1.37E-03	4.8	2.48E-01	4.1	2.98E-03	5.9
2	189	3167	2.36E-03	20.6	9.86E-05	21.0	2.29E-02	19.0	1.75E-04	22.7
3	222	4211	1.54E-04	19.2	3.50E-06	23.4	8.25E-04	23.3	9.51E-06	20.4
4	250	5180	2.03E-05	19.5	6.53E-07	16.2	1.27E-04	18.1	2.68E-06	12.2
5	243	5104	2.31E-05	17.8	5.47E-07	-24.4	9.28E-05	-42.5	8.92E-07	-150.4

Tab. 1: Example (E1) with $\varepsilon = 10^{-2}$.

where $\varepsilon > 0$ is a constant diffusion coefficient. We prescribe the Dirichlet boundary condition on $\partial\Omega$ and the source term g such that the exact solution has the form $u(x_1, x_2) = \big(c_1 + c_2(1 - x_1) + e^{-x_1/\varepsilon}\big)\big(c_1 + c_2(1 - x_2) + e$ with $c_1 = -e^{-1/\varepsilon}$, $c_2 = -1 - c_1$. The solution contains two boundary layers along $x_1 = 0$ and $x_2 = 0$, whose width is proportional to ε. Here we consider $\varepsilon = 10^{-2}$ and $\varepsilon = 10^{-3}$.

This example is suitable for the anisotropic adaptation since thin and long triangles can employed in the boundary layers. Tables 1 and 2 show the corresponding results for $\varepsilon = 10^{-2}$ and $\varepsilon = 10^{-3}$, respectively. We observe that the anisotropic adaptations requires significantly smaller N_{hp} than the isotropic one. Namely for $\varepsilon = 10^{-3}$, the difference is more essential.

Furthermore, Figures 6 and 7 show the final *hp*-grids with the details near origin and the horizontal boundary layer for $\varepsilon = 10^{-2}$ and $\varepsilon = 10^{-3}$, respectively. Here, each triangle of $\mathscr{T}_h$ is highlighted by the colour corresponding to the polynomial approximation degree. Obviously, the elements are aligned along the boundary layers. For the case $\varepsilon = 10^{-2}$, the "L^2-approach" leads to the slightly higher polynomial approximation degrees than the "L^∞-approach". For the case $\varepsilon = 10^{-3}$, both anisotropic techniques lead to similar *hp*-grids.

6.2 (E2): Nonlinear convection-diffusion equation with a corner singularity

We consider the scalar nonlinear convection-diffusion equation

$$-\nabla \cdot (\boldsymbol{K}(u)\nabla u) - \frac{\partial u^2}{\partial x_1} - \frac{\partial u^2}{\partial x_2} \quad = \quad g \quad \text{in } \Omega := (0,1)^2, \tag{6.3}$$

where $\boldsymbol{K}(u)$ is the nonsymmetric matrix given by

$$\boldsymbol{K}(u) = \varepsilon \begin{pmatrix} 2 + \arctan(u) & (2 - \arctan(u))/4 \\ 0 & (4 + \arctan(u))/2 \end{pmatrix}. \tag{6.4}$$

We put $\varepsilon = 10^{-3}$ and prescribe the Dirichlet boundary condition on $\partial\Omega$ and the source term g such that the exact solution is

$$u(x_1, x_2) = (x_1^2 + x_2^2)^{\alpha/2} x_1 x_2 (1 - x_1)(1 - x_2), \quad \alpha \in \mathbb{R}. \tag{6.5}$$

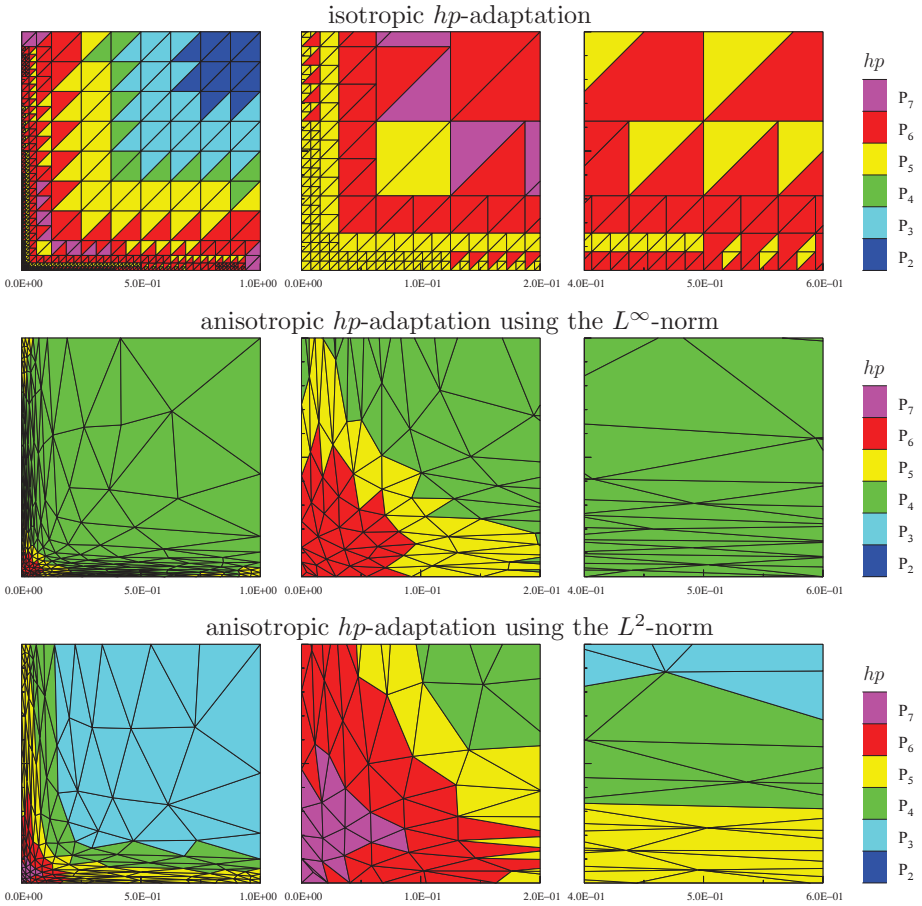

Fig. 6: Example (E1) given with $\varepsilon = 10^{-2}$: the final hp-meshes the total view (left), the detail around the origin (zoom 5) (centre) and the detail of the boundary layer (zoom 5) (right).

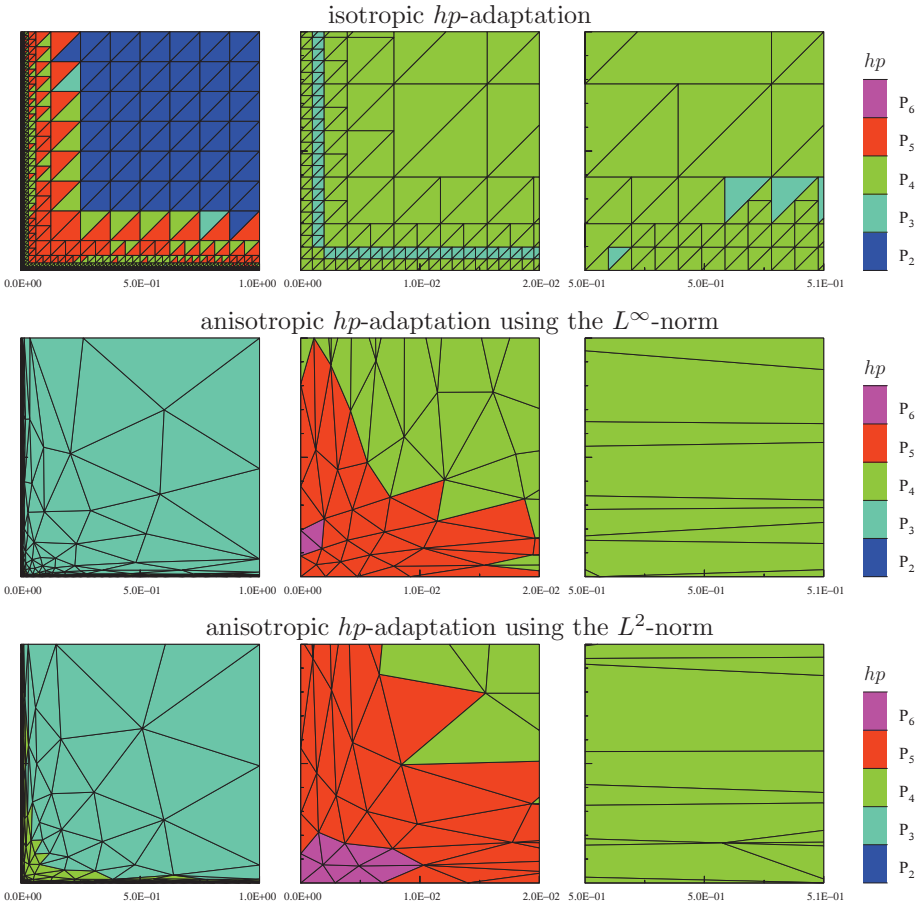

Fig. 7: Example (E1) with $\varepsilon = 10^{-3}$: the final hp-meshes the total view (left), the detail around the origin (zoom 50) (centre) and the detail of the boundary layer (zoom 100) (right).

isotropic *hp*-adaptation

ℓ	N_h	N_{hp}	$\|e_{hp}\|_{L^\infty}$	EOC	$\|e_{hp}\|_{L^2}$	EOC	$\|e_{hp}\|_{H^1}$	EOC	estim	EOC
0	128	384	1.71E-01	–	1.88E-02	–	5.78E-01	–	2.04E+01	–
1	128	768	2.29E-01	-0.8	1.76E-02	0.2	1.63E+01	-9.6	1.67E+01	0.6
2	146	1068	3.70E-01	-2.9	1.82E-02	-0.2	1.66E+01	-0.1	1.96E+01	-1.0
3	206	1806	4.97E-01	-1.1	1.58E-02	0.6	1.43E+01	0.6	2.09E+01	-0.3
4	350	3738	5.79E-01	-0.4	1.24E-02	0.7	1.23E+01	0.4	1.73E+01	0.5
5	824	9132	3.66E-01	1.0	7.98E-03	1.0	9.61E+00	0.5	1.33E+01	0.6
6	1832	20732	9.06E-02	3.4	2.98E-03	2.4	4.91E+00	1.6	6.63E+00	1.7
7	3716	42032	3.52E-02	2.7	6.20E-04	4.4	1.56E+00	3.2	2.01E+00	3.4
8	6380	72968	8.75E-03	5.0	7.94E-05	7.5	3.17E-01	5.8	3.99E-01	5.9
9	7814	103308	1.62E-03	9.7	9.64E-06	12.1	4.88E-02	10.8	6.28E-02	10.6
10	9548	138384	2.18E-04	13.7	4.38E-06	5.4	2.02E-02	6.0	2.52E-02	6.2

anisotropic *hp*-adaptation using the L^∞-norm

ℓ	N_h	N_{hp}	$\|e_{hp}\|_{L^\infty}$	EOC	$\|e_{hp}\|_{L^2}$	EOC	$\|e_{hp}\|_{H^1}$	EOC	estim	EOC
0	64	960	7.41E-01	–	1.71E-02	–	1.81E+01	–	3.08E-01	–
1	84	1260	6.50E-01	1.0	1.51E-02	0.9	1.60E+01	0.9	8.21E-01	-7.2
2	96	1440	5.90E-01	1.5	1.22E-02	3.2	1.36E+01	2.4	2.36E+00	-15.8
3	162	2430	4.92E-01	0.7	9.15E-03	1.1	1.00E+01	1.2	1.81E+00	1.0
4	201	3018	2.46E-01	6.4	4.17E-03	7.3	4.46E+00	7.5	7.28E-01	8.4
5	249	3725	6.75E-02	12.3	9.84E-04	13.7	1.03E+00	13.9	1.04E-01	18.5
6	350	5110	1.25E-02	10.7	8.36E-05	15.6	1.00E-01	14.7	9.51E-02	0.6
7	564	8207	9.52E-04	10.9	1.28E-05	7.9	1.41E-02	8.3	4.60E-03	12.8

anisotropic *hp*-adaptation using the L^2-norm

ℓ	N_h	N_{hp}	$\|e_{hp}\|_{L^\infty}$	EOC	$\|e_{hp}\|_{L^2}$	EOC	$\|e_{hp}\|_{H^1}$	EOC	estim	EOC
0	64	960	7.41E-01	–	1.71E-02	–	1.81E+01	–	1.10E-02	–
1	96	1440	6.72E-01	0.5	1.48E-02	0.7	1.60E+01	0.6	1.28E-02	-0.7
2	109	1635	5.64E-01	2.8	1.22E-02	3.0	1.36E+01	2.6	9.38E-03	4.8
3	137	2055	4.07E-01	2.9	8.72E-03	2.9	9.43E+00	3.2	4.77E-03	5.9
4	198	2976	2.05E-01	3.7	3.29E-03	5.3	3.55E+00	5.3	1.75E-03	5.4
5	256	3937	9.68E-02	5.4	1.14E-03	7.6	1.18E+00	7.9	2.91E-04	12.8
6	326	5057	1.39E-02	15.5	9.96E-05	19.5	1.09E-01	19.0	7.71E-05	10.6
7	491	7654	1.24E-03	11.7	1.62E-05	8.8	1.75E-02	8.8	9.74E-06	10.0

Tab. 2: Example (E1) with $\varepsilon = 10^{-3}$.

It is possible to show (see [4]) that $u \in H^\kappa(\Omega)$, $\kappa \in (0, 3+\alpha)$. Here, we choose $\alpha = -3/2$, which leads to the solution with a singularity at $x_1 = x_2 = 0$. Numerical examples presented in [18], carried out for a little different problem, show that this singularity avoids to achieve the order of convergence better than $O(h^{3/2})$ in the L^2-norm and $O(h^{1/2})$ in the H^1-seminorm for any polynomial approximation degree. Nevertheless, the exact solution is regular outside of the singularity. The exact solution of this example does not contain any boundary or interior layers, thus anisotropic adaptation can not give better results than the isotropic one.

Table 3 shows the corresponding results. We observe that the anisotropic adaptations require approximately the same N_{hp} as the isotropic one. Moreover, comparing both anisotropic adaptations we find that the "L^∞-approach" gives smaller $\|e_{hp}\|_{L^\infty}$ but larger $\|e_{hp}\|_{L^2}$ than the "L^2-approach" whereas $\|e_{hp}\|_{H^1}$ are the same. This indicates that the presented *hp*-adaptive method really optimizes the *hp*-mesh with respect to the given norm.

Finally, Figure 8 shows the final *hp*-grids with the details around the origin. We observe that the "L^2-approach" leads to the slightly higher polynomial approximation degrees than the "L^∞-approach".

6.3 (E3): Quasi-linear elliptic problem with a corner singularity

Similarly as in [28] (see also [27], [36]), we consider the quasi-linear elliptic problem

$$-\nabla \cdot (\mu(|\nabla u|)\nabla u) = f \quad \text{in } \Omega := (-1,1)^2 \setminus [0,1) \times (-1,0), \tag{6.6}$$

where $\mu(|\nabla u|) = 1 + e^{-|\nabla u|^2}$. We prescribe the Dirichlet boundary condition on $\partial\Omega$ and the source term g such that the exact solution is (in the polar coordinates)

$$u(r,\varphi) = r^{2/3}\sin(2\varphi/3). \tag{6.7}$$

We note that u has a corner singularity at $(0,0)$ and $u \notin H^2(\Omega)$.

isotropic *hp*-adaptation

ℓ	N_h	N_{hp}	$\|e_{hp}\|_{L^\infty}$	EOC	$\|e_{hp}\|_{L^2}$	EOC	$\|e_{hp}\|_{H^1}$	EOC	estim	EOC
0	128	384	6.10E-02	–	5.69E-03	–	3.76E-01	–	1.43E+00	–
1	128	756	4.82E-02	0.7	1.45E-03	4.0	1.83E-01	2.1	3.98E-01	3.8
2	128	900	8.79E-02	-6.9	1.29E-03	1.3	1.69E-01	0.9	1.98E-01	8.0
3	128	950	8.99E-02	-0.8	1.06E-03	7.2	1.32E-01	9.3	1.38E-01	13.6
4	134	1064	6.66E-02	5.3	4.39E-04	15.6	9.31E-02	6.1	9.78E-02	6.0
5	140	1166	4.66E-02	7.8	1.81E-04	19.4	6.61E-02	7.5	6.58E-02	8.7
6	152	1350	3.28E-02	4.8	1.01E-04	8.0	4.72E-02	4.6	4.63E-02	4.8
7	158	1432	2.49E-02	9.4	8.64E-05	5.2	3.96E-02	6.0	4.26E-02	2.8
8	161	1459	1.75E-02	39.4	8.28E-05	4.8	3.11E-02	27.2	3.42E-02	24.6
9	164	1490	1.24E-02	31.6	8.23E-05	0.6	2.26E-02	29.3	2.64E-02	23.8
10	170	1560	8.80E-03	14.9	8.22E-05	0.0	1.67E-02	13.0	2.15E-02	8.9
11	176	1633	6.23E-03	15.1	7.70E-05	2.8	1.28E-02	11.9	1.81E-02	7.4

anisotropic *hp*-adaptation using the L^∞-norm

ℓ	N_h	N_{hp}	$\|e_{hp}\|_{L^\infty}$	EOC	$\|e_{hp}\|_{L^2}$	EOC	$\|e_{hp}\|_{H^1}$	EOC	estim	EOC
0	64	960	1.09E-01	–	1.90E-03	–	2.04E-01	–	8.17E-02	–
1	33	495	1.18E-01	0.2	1.02E-03	-1.9	1.60E-01	-0.7	5.79E-02	-1.0
2	55	825	8.92E-02	1.1	4.68E-04	3.1	1.17E-01	1.2	7.40E-02	-1.0
3	57	855	5.88E-02	23.4	1.54E-04	62.6	8.32E-02	19.4	6.79E-02	4.9
4	72	1092	3.39E-02	4.5	4.37E-05	10.3	5.11E-02	4.0	3.66E-02	5.0
5	80	1242	1.78E-02	10.1	1.50E-05	16.6	3.02E-02	8.2	1.66E-02	12.3
6	80	1266	1.21E-02	39.9	1.12E-05	30.5	2.41E-02	23.3	1.31E-02	24.4
7	86	1386	1.20E-02	0.1	8.81E-06	5.3	2.19E-02	2.2	1.20E-02	2.0
8	83	1347	1.12E-02	-4.9	1.01E-05	9.4	2.00E-02	-6.1	8.23E-03	-25.7
9	90	1482	9.59E-03	3.2	7.56E-06	6.0	1.72E-02	3.2	7.23E-03	2.7
10	84	1404	8.47E-03	-4.6	9.75E-06	9.4	1.51E-02	-4.9	1.03E-02	13.2
11	85	1437	7.59E-03	9.3	1.49E-05	-36.1	1.36E-02	8.8	5.85E-03	48.3
12	89	1503	6.25E-03	8.7	1.36E-05	4.2	1.15E-02	7.4	4.53E-03	11.4

anisotropic *hp*-adaptation using the L^2-norm

ℓ	N_h	N_{hp}	$\|e_{hp}\|_{L^\infty}$	EOC	$\|e_{hp}\|_{L^2}$	EOC	$\|e_{hp}\|_{H^1}$	EOC	estim	EOC
0	64	960	1.09E-01	–	1.90E-03	–	2.04E-01	–	1.22E-03	–
1	48	738	1.07E-01	-0.2	7.94E-04	-6.6	1.40E-01	-2.9	8.88E-04	-2.4
2	68	1080	7.24E-02	2.0	2.84E-04	5.4	1.06E-01	1.4	2.39E-04	6.9
3	75	1269	5.04E-02	4.5	9.03E-05	14.2	6.84E-02	5.5	7.26E-05	14.8
4	71	1227	4.08E-02	-12.6	4.34E-05	-43.6	5.57E-02	-12.3	4.59E-05	-27.3
5	75	1377	2.89E-02	6.0	1.79E-05	15.3	3.98E-02	5.8	3.44E-05	5.0
6	74	1374	2.44E-02	359.6	9.40E-06	1404.1	3.32E-02	389.7	2.71E-05	544.7
7	69	1305	1.93E-02	-9.3	6.58E-06	-13.9	2.59E-02	-9.6	4.49E-05	19.6
8	73	1413	1.56E-02	5.3	4.71E-06	8.4	2.10E-02	5.3	3.83E-05	4.0
9	77	1549	1.21E-02	5.6	3.85E-06	4.4	1.64E-02	5.4	3.77E-05	0.4
10	81	1685	1.07E-02	2.8	2.82E-06	7.4	1.45E-02	2.9	4.05E-05	-1.7
11	84	1815	8.19E-03	7.3	1.81E-06	11.9	1.11E-02	7.3	2.03E-05	18.5

Tab. 3: Example (E2).

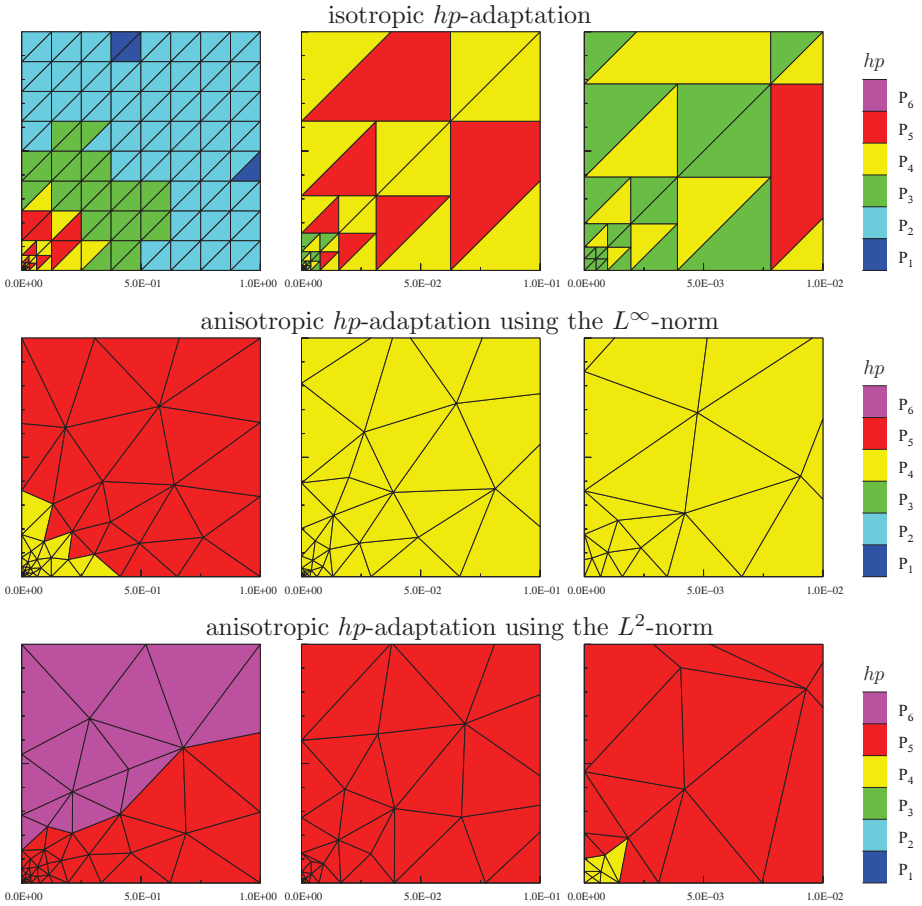

Fig. 8: Example (E2): the final *hp*-meshes the total view (left) and the details around the origin singularity, zoom 10 (centre) and 100 (right).

isotropic *hp*-adaptation

ℓ	N_h	N_{hp}	$\|e_{hp}\|_{L^\infty}$	EOC	$\|e_{hp}\|_{L^2}$	EOC	$\|e_{hp}\|_{H^1}$	EOC	estim	EOC
0	96	288	2.54E-02	–	6.60E-03	–	1.48E-01	–	2.32E-01	–
1	96	576	1.38E-02	1.8	1.83E-03	3.7	5.55E-02	2.8	7.59E-02	3.2
2	96	960	2.07E-02	-1.6	1.63E-03	0.4	3.86E-02	1.4	3.73E-02	2.8
3	96	1255	1.79E-02	1.1	1.17E-03	2.5	2.85E-02	2.3	2.10E-02	4.3
4	96	1387	1.56E-02	2.7	8.14E-04	7.2	2.32E-02	4.1	1.27E-02	9.9
5	96	1499	1.43E-02	2.3	5.84E-04	8.6	2.02E-02	3.6	8.21E-03	11.3
6	96	1579	1.36E-02	1.8	4.30E-04	11.8	1.80E-02	4.3	5.56E-03	15.0
7	96	1685	1.30E-02	1.5	3.24E-04	8.8	1.63E-02	3.1	3.90E-03	10.9
8	108	2285	6.60E-03	4.5	1.20E-04	6.5	1.05E-02	2.9	2.60E-03	2.7
9	138	3571	4.99E-03	1.3	6.24E-05	2.9	7.26E-03	1.7	2.17E-03	0.8
10	168	4395	3.84E-03	2.5	3.67E-05	5.1	5.17E-03	3.3	2.03E-03	0.7
11	183	4622	2.55E-03	16.1	1.75E-05	29.2	3.72E-03	13.1	1.97E-03	1.0
12	198	4707	1.67E-03	50.1	1.17E-05	47.4	2.79E-03	33.5	2.02E-03	-3.1
13	189	4471	9.73E-04	-21.1	4.09E-06	-41.2	1.86E-03	-15.9	1.39E-03	-14.8
14	210	4811	6.15E-04	12.6	2.51E-06	13.4	1.32E-03	9.4	1.04E-03	8.0
15	237	5217	3.88E-04	11.3	1.80E-06	8.1	8.36E-04	11.2	6.66E-04	11.0
16	252	5499	2.44E-04	17.8	1.66E-06	3.2	5.33E-04	17.4	4.34E-04	16.6
17	267	5747	1.54E-04	20.9	1.63E-06	0.7	3.45E-04	19.6	2.95E-04	17.4
18	282	5990	9.69E-05	22.0	1.62E-06	0.4	2.32E-04	18.9	2.17E-04	14.6
19	297	6231	6.11E-05	23.3	1.55E-06	2.1	1.65E-04	17.2	1.72E-04	11.6

anisotropic *hp*-adaptation using the L^∞-norm

ℓ	N_h	N_{hp}	$\|e_{hp}\|_{L^\infty}$	EOC	$\|e_{hp}\|_{L^2}$	EOC	$\|e_{hp}\|_{H^1}$	EOC	estim	EOC
0	96	1440	1.79E-02	–	1.16E-03	–	2.85E-02	–	5.54E-03	–
1	190	2970	1.12E-02	1.3	4.44E-04	2.7	1.78E-02	1.3	3.37E-03	1.4
2	234	3678	6.25E-03	5.4	1.54E-04	9.9	1.06E-02	4.9	2.74E-03	1.9
3	272	4308	3.41E-03	7.7	5.88E-05	12.2	6.60E-03	6.0	9.68E-04	13.2
4	284	4592	2.63E-03	8.1	3.43E-05	17.0	5.04E-03	8.5	1.39E-03	-11.4
5	313	5175	1.61E-03	8.3	1.44E-05	14.5	3.37E-03	6.7	8.50E-04	8.2
6	333	5578	9.67E-04	13.5	5.20E-06	27.1	2.19E-03	11.5	1.92E-03	-21.7
7	341	5850	7.68E-04	9.7	3.15E-06	21.0	1.60E-03	13.3	4.59E-04	60.2
8	351	6181	4.86E-04	16.6	1.27E-06	32.9	1.08E-03	14.0	7.91E-04	-19.8
9	353	6395	2.44E-04	41.8	4.70E-07	60.7	8.45E-04	15.2	7.87E-04	0.2
10	351	6423	2.38E-04	9.2	3.24E-07	120.3	5.76E-04	126.2	3.07E-04	307.6
11	358	6720	1.81E-04	12.0	1.95E-07	22.5	4.42E-04	11.7	3.94E-04	-11.0
12	360	6796	1.17E-04	57.9	1.09E-07	77.9	3.57E-04	28.4	2.93E-04	39.3
13	348	6691	8.79E-05	-37.4	7.18E-08	-53.6	2.97E-04	-23.9	1.38E-04	-97.6
14	350	6870	6.89E-05	18.0	5.65E-08	17.8	2.49E-04	13.1	2.38E-04	-39.9
15	350	6893	8.62E-05	-48.3	6.58E-08	-31.0	2.18E-04	28.6	1.17E-04	157.6

anisotropic *hp*-adaptation using the L^2-norm

ℓ	N_h	N_{hp}	$\|e_{hp}\|_{L^\infty}$	EOC	$\|e_{hp}\|_{L^2}$	EOC	$\|e_{hp}\|_{H^1}$	EOC	estim	EOC
0	96	1440	1.79E-02	–	1.16E-03	–	2.85E-02	–	1.68E-04	–
1	292	5352	1.01E-02	0.9	3.52E-04	1.8	1.67E-02	0.8	6.68E-05	1.4
2	314	6052	5.20E-03	10.8	1.04E-04	19.9	8.60E-03	10.7	1.49E-05	24.3
3	331	7264	2.65E-03	7.4	2.89E-05	14.0	5.13E-03	5.7	7.62E-06	7.4
4	287	6979	1.44E-03	-31.0	1.14E-05	-47.1	3.45E-03	-20.1	3.77E-06	-35.7
5	252	6815	1.06E-03	-27.0	5.56E-06	-62.7	2.38E-03	-32.7	1.31E-06	-92.7
6	221	6337	8.11E-04	-7.4	2.39E-06	-23.5	1.69E-03	-9.4	2.03E-06	12.2
7	228	6856	5.78E-04	8.6	9.70E-07	22.8	1.14E-03	10.0	4.11E-07	40.5
8	218	6880	3.67E-04	813.1	5.79E-07	926.8	8.09E-04	607.6	2.78E-07	704.7
9	206	6792	3.28E-04	-18.2	4.02E-07	-59.2	6.05E-04	-47.0	5.25E-07	103.4
10	193	6420	2.27E-04	-13.1	2.31E-07	-19.8	4.91E-04	-7.5	9.81E-07	22.4
11	221	7444	1.84E-04	2.8	1.09E-07	10.1	4.01E-04	2.8	4.63E-07	10.1
12	212	7224	1.28E-04	-23.0	6.36E-08	-34.2	3.26E-04	-13.0	6.30E-07	19.5
13	222	7658	1.09E-04	5.4	3.47E-08	20.8	2.76E-04	5.7	5.19E-07	6.6
14	218	7732	8.72E-05	50.2	1.84E-08	140.2	2.63E-04	11.7	4.18E-07	47.1
15	219	7904	7.48E-05	13.8	1.36E-08	26.8	2.49E-04	4.8	4.05E-07	2.9
16	219	8041	7.10E-05	6.5	2.15E-08	-59.1	1.56E-04	59.7	3.61E-07	14.6

Tab. 4: Example (E3).

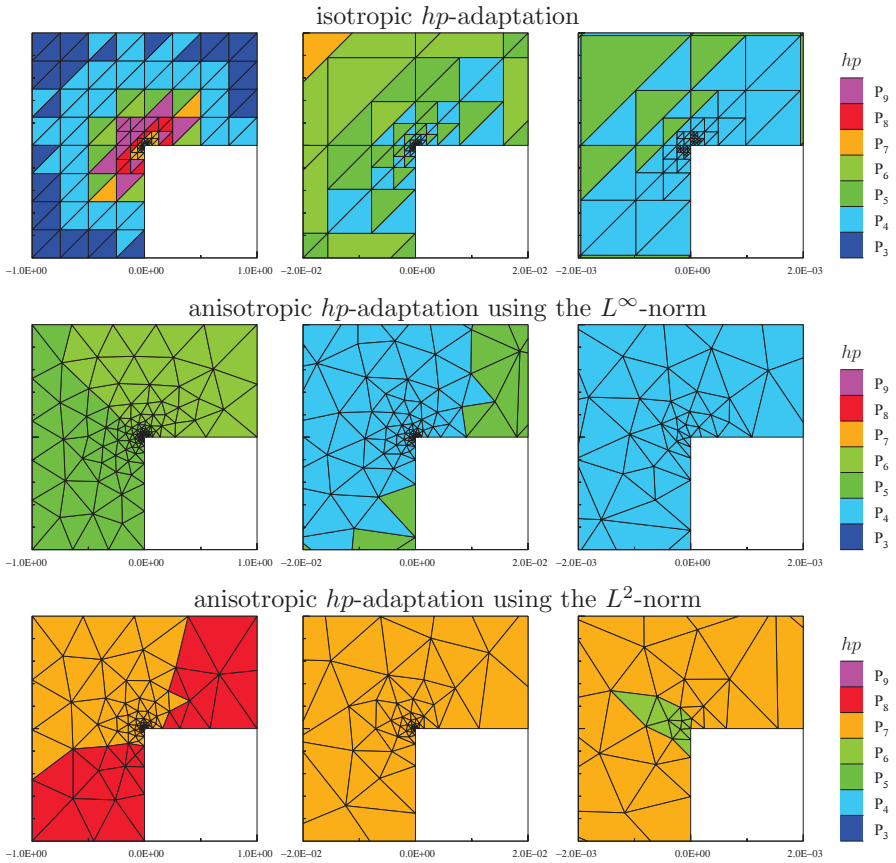

Fig. 9: Example (E3): the final *hp*-meshes the total view (left) and the details around the origin singularity, zoom 50 (centre) and 500 (right).

Table 4 shows the corresponding results. We observe that the anisotropic adaptation requires a little more N_{hp} than the isotropic case. Furthermore, Figure 9 shows the final *hp*-grids with the details near origin. We observe very fine refinement near the singularity for all cases. The 'L^2-approach" leads again to the higher polynomial approximation degrees than the "L^∞-approach".

6.4 (E4): Double curved interior layers problem

We consider a linear convection-dominated problem [32, Example 6.2]

$$-\varepsilon\triangle u + b_1\frac{\partial u}{\partial x_1} + b_2\frac{\partial u}{\partial x_2} = 0 \quad \text{in } \Omega := (0,1)^2, \tag{6.8}$$

where $\varepsilon = 10^{-6}$ and $(b_1, b_2) = (-x_2, x_1)$, is the velocity field with curved characteristics. We prescribe the homogeneous Neumann data at the outflow part $\partial\Omega_N = \{0\}\times(0,1)$ and the discontinuous Dirichlet data $u = 1$ at $(x_1, x_2) \in (\frac{1}{3}, \frac{2}{3})\times\{0\}$ and $u = 0$ elsewhere on $\partial\Omega_D := \partial\Omega \setminus \partial\Omega_N$. Then this discontinuous profile is basically transported along the characteristic curves leading to sharp characteristic interior layers.

We investigate the ability of the proposed anisotropic *hp*-algorithm to capture the sharp curved interior layers. We present the solution obtained by the anisotropic *hp*-adaptive technique using the estimate of the interpolation error function in the L^2-norm. Figure 10 shows the final *hp*-grid with the zooms of both interior layer. Figure 11 shows the isolines of the solution obtained on the final grid and the diagonal cut of the approximate solution along $x_2 = x_1$. We observe a sharp

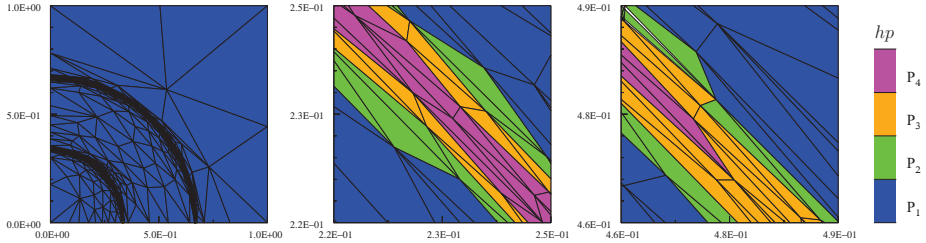

Fig. 10: Example (E4), the total view (left) and the details near the first (centre) and the second (right) interior layers with zoom 33.

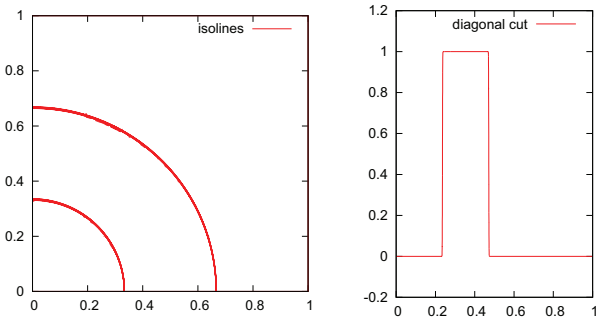

Fig. 11: Example (E4), the isolines of the solution (left) with the cut along $x_2 = x_1$ (right).

capturing of the both interior layers without any overshoots and undershoots of the solution. We recall that any stabilization technique (see, e.g., [31]) was not used in the DG solver. Similar results can be obtain also for $q = \infty$.

6.5 (E5): Triple curved interior layers problem

Here, we consider a generalization of example (E4), namely, the linear convection-dominated problem (6.8) with $\Omega := (0,2) \times (0,1)$, $\varepsilon = 10^{-6}$, and the velocity field $(b_1, b_2) = (x_2, (1-x_1)^2)$. We prescribe the homogeneous Neumann data at the outflow part $\partial\Omega_N := \{2\} \times (0,1) \cup (0,2) \times \{1\}$ and the discontinuous Dirichlet data

$$u = \begin{cases} 1 & x_1 \in (\frac{1}{8}, \frac{1}{2}),\ x_2 = 0 \\ 2 & x_1 \in (\frac{1}{2}, \frac{3}{4}),\ x_2 = 0 \\ 0 & \text{elsewhere on } \partial\Omega_D := \partial\Omega \setminus \partial\Omega_N. \end{cases} \tag{6.9}$$

Then this discontinuous profile is basically transported along the characteristic curves leading to sharp characteristic interior layers. Figure 12 shows the sketch of the exact solution.

We present the solution obtained by the adaptive technique using the estimate in the L^2-norm. Figure 13 shows the final *hp*-grid with the zooms of all interior layers near $\partial\Omega_N$. Furthermore, Figure 14, shows the isolines of the solution obtained on the final grid and the vertical cut of the approximate solution along $x_1 = 1$. Again, due to a strong mesh refinement, we do not observe any unphysical oscillations of the approximate solution. Similar results can be obtain also for $q = \infty$.

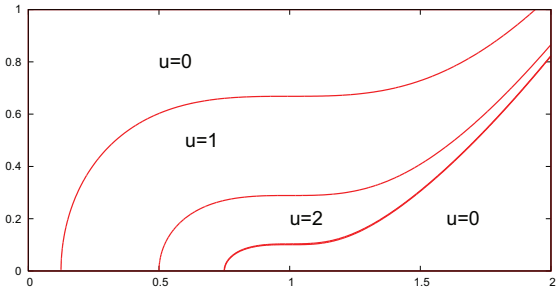

Fig. 12: Example (E5), sketch of the exact solution.

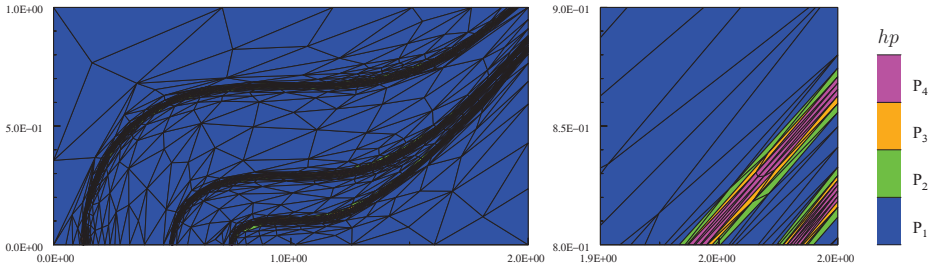

Fig. 13: Example (E5), the total view (left) and the detail of the right bottom corner (right).

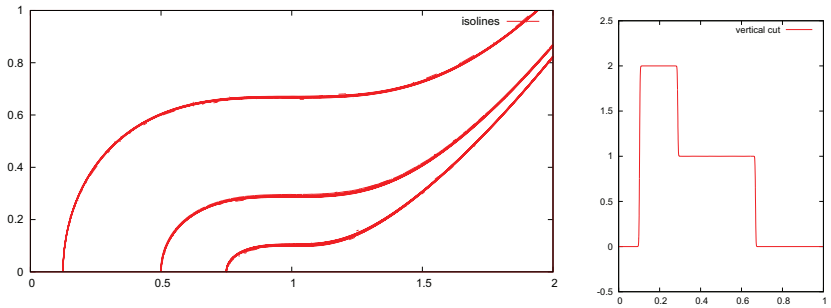

Fig. 14: Example (E5), the isolines of the solution (left) and the cut of the solution along $x_1 = 1$ (right).

7 Conclusion and outlook

We developed the technique which generates anisotropic *hp*-grids based on the interpolation error estimates in the L^q-norm, $q \in [1, \infty]$. These grids can be employed for the numerical solution of partial differential equations with the aid of the discontinuous Galerkin method. Although the presented numerical examples demonstrate the efficiency of this approach in comparison to the isotropic *hp*-adaptive method, we have no information about the computational error. We suppose that it will be possible to combine this approach with some a posteriori error estimation technique. Particularly, we expect that a posteriori error estimate gives us the information about the size of the error and the presented technique about the anisotropy of the elements. This is the subject of the future research. Moreover, it is demanding to extend this approach also to time-dependent problems and to more challenging problems, e.g., from the computational fluid dynamics.

Appendix

We prove Lemma 3.13, i.e.,

$$S(\delta) > S(1) = 2\pi \quad \forall \delta > 1, \tag{7.1}$$

where

$$S(\delta) := \int_{t=0}^{2\pi} \left(\delta \cos^2 t + \frac{1}{\delta} \sin^2 t \right)^s \mathrm{d}t, \qquad \delta \geq 1,\ s \geq 1. \tag{7.2}$$

Proof. We set $z(t) := \delta \cos^2 t + 1/\delta \sin^2 t$. For $\delta = 1$, we have $z(t) = 1$ on $[0, 2\pi]$ and thus $S(1) = 2\pi$.

Let $\delta > 1$. The function $z(t)$ is viewed in Figure 15, left. First, we consider the case $s = 1$. Using identity $\int_0^{2\pi} \cos^2(t)\,\mathrm{d}t = \int_0^{2\pi} \sin^2(t)\,\mathrm{d}t = \pi$, we have

$$S(\delta) = \int_0^{2\pi} \left(\delta \cos^2 t + 1/\delta \sin^2 \right) \mathrm{d}t = \pi(\delta + 1/\delta) > 2\pi \quad \forall \delta > 1, \tag{7.3}$$

where the last inequality follows from the inequality $(\sqrt{\delta} - 1/\sqrt{\delta})^2 > 0\ \forall \delta > 1$.

Let $s > 1$. The function $z(t)$ is periodic with the period $\pi/2$, hence we consider the integral of $z(t)$ over $[0, \pi/2]$. Due to the identities $\cos^2(\pi/2 - t) = \sin^2 t$ and $\sin^2(\pi/2 - t) = \cos^2 t$, we have

$$\int_0^{\frac{\pi}{2}} z(t)^s\,\mathrm{d}t = \int_0^{\frac{\pi}{4}} \left(z(t)^s + z(\pi/2 - t)^s \right) \mathrm{d}t = \int_0^{\frac{\pi}{4}} \tilde{z}(t)\,\mathrm{d}t, \tag{7.4}$$

where

$$\tilde{z}(t) := \left(\delta \cos^2 t + \frac{1}{\delta} \sin^2 t \right)^s + \left(\delta \sin^2 t + \frac{1}{\delta} \cos^2 t \right)^s, \tag{7.5}$$

see Figure 15, right. We show that $\tilde{z}(t) > 2\ \forall t \in [0, \pi/4]$. Obviously,

$$\begin{aligned} \tilde{z}(0) &= \delta^s + \frac{1}{\delta^s} = \left(\delta^s - 2 + \frac{1}{\delta^s} \right) + 2 = \left(\sqrt{\delta^s} - \frac{1}{\sqrt{\delta^s}} \right)^2 + 2 > 2 \quad \forall \delta > 1\, \forall s > 1, \\ \tilde{z}(\pi/4) &= \left(\frac{\delta}{2} + \frac{1}{2\delta} \right)^s + \left(\frac{\delta}{2} + \frac{1}{2\delta} \right)^s = 2\frac{1}{2^s} \left(\delta + \frac{1}{\delta} \right)^s > 2 \quad \forall \delta > 1, \end{aligned} \tag{7.6}$$

where the last inequality follows from the implications

$$\left(\sqrt{\delta} - \frac{1}{\sqrt{\delta}} \right)^2 > 0 \ \Rightarrow\ \delta + \frac{1}{\delta} > 2 \ \Rightarrow\ \left(\delta + \frac{1}{\delta} \right)^s > 2^s \ \Rightarrow\ \frac{1}{2^s} \left(\delta + \frac{1}{\delta} \right)^s > 1.$$

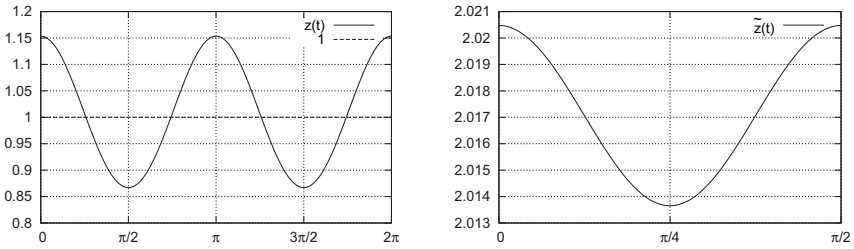

Fig. 15: Illustration for the proof of Lemma 3.13, the function $z(t)$ (left) and function $\tilde{z}(t)$ for $\delta = 1.1$ and $s = 1.5$.

Further, we show that $\tilde{z}(t)$ is non-increasing on $[0, \pi/4]$. Hence, we have to verify the inequality $\frac{\mathrm{d}}{\mathrm{d}t}\tilde{z}(t) \leq 0$ for $t \in [0, \pi/4]$, particularly

$$\begin{aligned}\frac{\mathrm{d}}{\mathrm{d}t}\tilde{z}(t) = \; & s\left(\delta\cos^2 t + \frac{1}{\delta}\sin^2 t\right)^{s-1}\left(-2\delta\cos t\sin t + \frac{2}{\delta}\sin t\cos t\right) \\ & + s\left(\delta\sin^2 t + \frac{1}{\delta}\cos^2 t\right)^{s-1}\left(2\delta\sin t\cos t - \frac{2}{\delta}\sin t\cos t\right) \\ = \; & s\sin(2t)\left(\frac{1}{\delta} - \delta\right)\left[\left(\delta\cos^2 t + \frac{1}{\delta}\sin^2 t\right)^{s-1} - \left(\delta\sin^2 t + \frac{1}{\delta}\cos^2 t\right)^{s-1}\right] \leq \; 0.\end{aligned} \tag{7.7}$$

This inequality is satisfied trivially for $t = 0$. Let $t > 0$. Dividing (7.7) by $s\sin(2t)(1/\delta - \delta) < 0$ for $t \in (0, \pi/4)$ and $\delta > 1$, we obtain

$$\begin{aligned} & \left(\delta\cos^2 t + \frac{1}{\delta}\sin^2 t\right)^{s-1} \geq \left(\delta\sin^2 t + \frac{1}{\delta}\cos^2 t\right)^{s-1} \\ \iff \quad & \delta\cos^2 t + \frac{1}{\delta}\sin^2 t \;\geq\; \delta\sin^2 t + \frac{1}{\delta}\cos^2 t \\ \iff \quad & \left(\delta - \frac{1}{\delta}\right)\left(\cos^2 t - \sin^2 t\right) \;\geq\; 0, \end{aligned}$$

which is true for $t \in (0, \pi/4)$ and $\delta > 1$. Moreover, we have $\frac{\mathrm{d}}{\mathrm{d}t}\tilde{z}(0) = \frac{\mathrm{d}}{\mathrm{d}t}\tilde{z}(\pi/4) = 0$. Hence, the function $\tilde{z}(t)$ is non-increasing on $(0, \pi/4)$ and attains its minimum for $t = \pi/4$. Using (7.6), we conclude that $\tilde{z}(t) > 2$ on $[0, \pi/4]$ which together with (7.4) implies

$$\int_0^{\frac{\pi}{2}} z(t)^s \,\mathrm{d}t = \int_0^{\frac{\pi}{4}} \tilde{z}(t)\,\mathrm{d}t > \int_0^{\frac{\pi}{4}} 2\,\mathrm{d}t = \frac{\pi}{2}.$$

Similarly, we can prove that $\int_{(\ell-1)\pi/2}^{\ell\pi/2} z(t)\,\mathrm{d}t > \pi/2,\ \ell = 2, 3, 4$, which gives (7.1). □

References

[1] J. C. Aguilar and J. B. Goodman. Anisotropic mesh refinement for finite element methods based on error reduction. *J. Comput. Appl. Math.*, 193(2):497 – 515, 2006.

[2] D. Ait-Ali-Yahia, G. Baruzzi, W. G. Habashi, M. Fortin, J. Dompierre, and M. Vallet. Anisotropic mesh adaptation: towards user-independent, mesh-independent and solver-independent CFD. II. Structured grids. *Internat. J. Numer. Methods Fluids*, 39:657–673, 2002.

[3] T. Apel. *Anisotropic Finite Elements: Local Estimates and Applications*. Teubner, Stuttgart - Leipzig, 1999.

[4] I. Babuška and M. Suri. The *p*- and *hp*- versions of the finite element method. An overview. *Comput. Methods Appl. Mech. Eng.*, 80:5–26, 1990.

[5] I. Babuška and M. Suri. The $p-$ and $hp-$FEM a survey. *SIAM Review*, 36:578–632, 1994.

[6] W. Cao. Anisotropic measures of third order derivatives and the quadratic interpolation error on triangular elements. *SIAM J. Sci. Comput.*, 29(2):756–781, 2007.

[7] W. Cao. An interpolation error estimate in R^2 based on the anisotropic measures of higher order derivatives. *Math. Comp.*, 77(261):265–286, 2008.

[8] L. Chen, P. Sun, and J. Xu. Optimal anisotropic meshes for minimizing interpolation errors in L^p-norm. *Math. Comp.*, 76:179–204, 2007.

[9] P. G. Ciarlet. *The Finite Elements Method for Elliptic Problems*. North-Holland, Amsterdam, New York, Oxford, 1979.

[10] C. Clavero, J. L. Gracia, and J. C. Jorge. A uniformly convergent alternating direction (HODIE) finite difference scheme for 2D time-dependent convection-diffusion problems. *IMA J. Numer. Anal.*, 26:155–172, 2006.

[11] C. N. Dawson, S. Sun, and M. F. Wheeler. Compatible algorithms for coupled flow and transport. *Comput. Meth. Appl. Mech. Engng.*, 193:2565–2580., 2004.

[12] L. Demkowicz, W. Rachowicz, and Ph. Devloo. A fully automatic *hp*-adaptivity. *J. Sci. Comput.*, 17(1-4):117–142, 2002.

[13] V. Dolejší. Anisotropic mesh adaptation for finite volume and finite element methods on triangular meshes. *Comput. Vis. Sci.*, 1(3):165–178, 1998.

[14] V. Dolejší. *ANGENER – software package*. Charles University Prague, Faculty of Mathematics and Physics, 2000. http://www.karlin.mff.cuni.cz/dolejsi/angen.html.

[15] V. Dolejší. *Adaptive higher order methods for compressible flow*, chapter Anisotropic mesh adaptation method. Charles University Prague, Faculty of Mathematics and Physics, 2003. Habilitation thesis.

[16] V. Dolejší. Analysis and application of IIPG method to quasilinear nonstationary convection-diffusion problems. *J. Comp. Appl. Math.*, 222:251–273, 2008.

[17] V. Dolejší. *hp*-DGFEM for nonlinear convection-diffusion problems. *Math. Comput. Simul.*, 87:87–118, 2013.

[18] V. Dolejší, M. Feistauer, V. Kučera, and V. Sobotíková. An optimal $L^\infty(L^2)$-error estimate of the discontinuous Galerkin method for a nonlinear nonstationary convection-diffusion problem. *IMA J. Numer. Anal.*, 28(3):496–521, 2008.

[19] V. Dolejší and J. Felcman. Anisotropic mesh adaptation and its application for scalar diffusion equations. *Numer. Methods Partial Differ. Equations*, 20:576–608, 2004.

[20] V. Dolejší and H.-G. Roos. BDF-FEM for parabolic singularly perturbed problems with exponential layers on layer-adapted meshes in space. *Neural Parallel Sci. Comput.*, 18(2):221–235, 2010.

[21] J. Dompierre, M.-G. Vallet, Y. Bourgault, M. Fortin, and W. G. Habashi. Anisotropic mesh adaptation: towards user-independent, mesh-independent and solver-independent CFD. Part III. unstructured meshes. *Int. J. Numer. Methods Fluids*, 39(8):675–702, 2002.

[22] T. Eibner and J. M. Melenk. An adaptive strategy for *hp*-FEM based on testing for analyticity. *Comput. Mech.*, 39(5):575–595, 2007.

[23] P. J. Frey and F. Alauzet. Anisotropic mesh adaptation for CFD computations. *Comput. Methods Appl. Mech. Engrg.*, 194:5068–5082, 2005.

[24] E. H. Georgoulis. *hp*-version interior penalty discontinuous Galerkin finite element methods on anisotropic meshes. *Int. J. Numer. Anal. Model.*, 3(1):52–79, 2006.

[25] S. Giani and P. Houston. Anisotropic *hp*-adaptive discontinuous Galerkin finite element methods for compressible fluid flows. *Int. J. Numer. Anal. Model.*, 9(4):928–949, 2012.

[26] W. G. Habashi, J. Dompierre, Y. Bourgault, D. Ait-Ali-Yahia, M. Fortin, and M.-G. Vallet. Anisotropic mesh adaptation: towards user-independent, mesh-independent and solver-independent CFD. Part I: general principles. *Int. J. Numer. Methods Fluids*, 32(6):725–744, 2000.

[27] P. Houston, D. Schötzau, and T. P. Wihler. Energy norm a posteriori error estimation of *hp*-adaptive discontinuous Galerkin methods for elliptic problems. *Math. Models Methods Appl. Sci.*, 17(1):33–62, 2007.

[28] P. Houston, E. Süli, and T. P. Wihler. A posteriori error analysis of *hp*-version discontinuous Galerkin finite element methods for second-order quasilinear elliptic problems. *IMA J. Numer. Anal.*, 28:245–273, 2008.

[29] P. Houston and E. Sülli. A note on the design of *hp*–adaptive finite element methods for elliptic partial differential equations. *Comput. Methods Appl. Mech. Engrg.*, 194:229–243, 2005.

[30] J. Hozman. *Discontinuous Galerkin Method for Convection-Diffusion Problems*. PhD thesis, Charles University Prague, Faculty of Mathematics and Physics, 2009.

[31] V. John and P. Knobloch. On spurious oscillations at layer diminishing (SOLD) methods for convection–diffusion equations: Part I – A review. *Comput. Methods Appl. Mech Engrg.*, 196:2197–2215, 2007.

[32] T. Knopp, G. Lube, and G. Rapin. Stabilized finite element methods with shock capturing for advection–diffusion problems. *Comput. Methods Appl. Mech. Engrg.*, 191:2997–3013, 2002.

[33] P. Laug and H. Borouchaki. *BL2D-V2: isotropic or anisotropic 2D mesher*. INRIA, 2002. https://www.rocq.inria.fr/gamma/Patrick.Laug/logiciels/bl2d-v2/INDEX.html.

[34] T. Leicht and R. Hartmann. Anisotropic mesh refinement for discontinuous Galerkin methods in two-dimensional aerodynamic flow simulations. *Int. J. Numer. Meth. Fluids*, 56(11):2111–2138, 2008.

[35] J. M. Melenk. *hp-finite element methods for singular perturbations*, volume 1796 of *Lecture Notes in Mathematics*. Springer-Verlag, Berlin, 2002.

[36] J. M. Melenk and B. I. Wohlmuth. On residual-based a posteriori error estimation in *hp*-FEM. *Adv. Comput. Math.*, 15:311–331, 2001.

[37] C. Schwab. *p- and hp-Finite Element Methods*. Clarendon Press, Oxford, 1998.

[38] R. B. Simpson. Anisotropic mesh transformations and optimal error control. *Applied Numer. Math.*, 14:183–198, 1994.

[39] P. Šolín and L. Demkowicz. Goal-oriented *hp*-adaptivity for elliptic problems. *Comput. Methods Appl. Mech. Engrg.*, 193:449–468, 2004.

[40] S. Sun. *Discontinuous Galerkin methods for reactive transport in porous media*. PhD thesis, The University of Texas, Austin, 2003.

[41] T. P. Wihler, O. Frauenfelder, and C. Schwab. Exponential convergence of the *hp*-DGFEM for diffusion problems. *Comput. Math. Appl.*, 46:183–205, 2003.

[42] O. C. Zienkiewicz and J. Wu. Automatic directional refinement in adaptive analysis of compressible flows. *Int. J. Numer. Methods Engrg.*, 37(13):2189–2210, 1994.